AD-A037 183 RENSSELAER POLYTECHNIC INST TROY N Y DEPT OF MECHANI--ETC F/G 11/8
MEASUREMENT OF PROPERTIES AND RESPONSE FUNCTIONS OF LIQUID LUBR--ETC(U)
AUG 76 M H BIRNBOIM F33615-75-C-5105

UNCLASSIFIED AFML-TR-76-146 NL

| OF |
AD
A037183

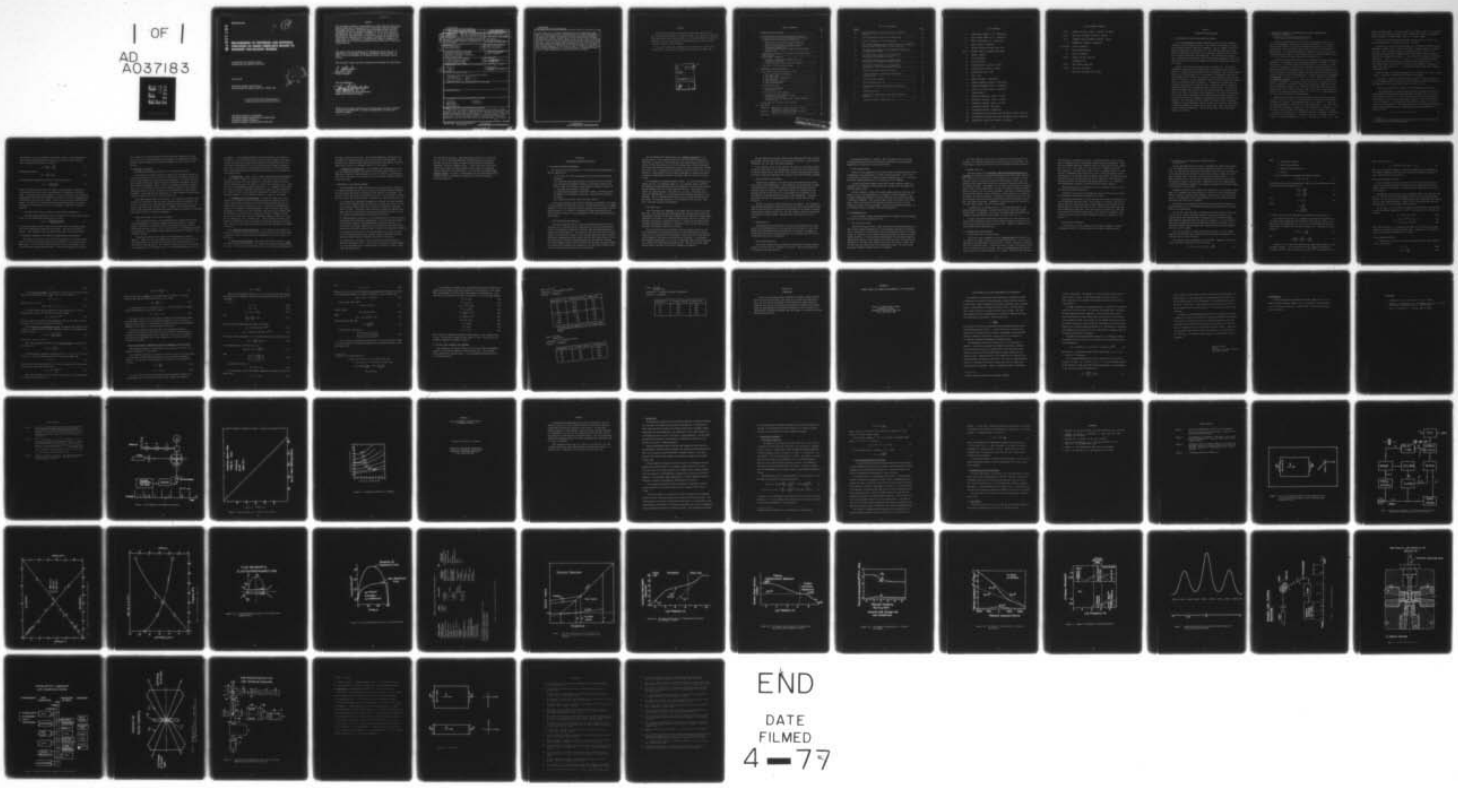

END

DATE
FILMED
4-77

AD A037183

AFML-TR-76-146

12

# MEASUREMENT OF PROPERTIES AND RESPONSE FUNCTIONS OF LIQUID LUBRICANTS RELATED TO TRANSIENT VISCOELASTIC REGIMES

*LABORATORY FOR VISCOELASTICITY*
*RENSSELAER POLYTECHNIC INSTITUTE*

DDC
MAR 22 1977
C

AUGUST 1976

TECHNICAL REPORT AFML-TR-76-146
FINAL REPORT FOR PERIOD APRIL 1975 - MARCH 1976

Approved for public release; distribution unlimited

AIR FORCE MATERIALS LABORATORY
AIR FORCE WRIGHT AERONAUTICAL LABORATORIES
AIR FORCE SYSTEMS COMMAND
WRIGHT-PATTERSON AIR FORCE BASE, OHIO 45433

61102F

## NOTICE

When Government drawings, specifications, or other data are used for any purpose other than in connection with a definitely related Government procurement operation, the United States Government thereby incurs no responsibility nor any obligation whatsoever; and the fact that the government may have formulated, furnished, or in any way supplied the said drawings, specifications, or other data, is not to be regarded by implication or otherwise as in any manner licensing the holder or any other person or corporation, or conveying any rights or permission to manufacture, use, or sell any patented invention that may in any way be related thereto.

This report has been reviewed by the Information Office (IO) and is releasable to the National Technical Information Service (NTIS). At NTIS, is will be available to the general public, including foreign nations.

This technical report has been reviewed and is approved for publication.

FREDRICK C. BROOKS
Project Engineer

FOR THE COMMANDER

LARRY L EHRENBACHER, Maj., USAF
Chief, Lubricants and Tribology Branch
Nonmetallic Materials Division

Copies of this report should not be returned unless return is required by security consideration, contractual obligations, or notice on a specific document.

AIR FORCE - 4 FEBRUARY 77 - 250

UNCLASSIFIED

SECURITY CLASSIFICATION OF THIS PAGE (When Data Entered)

(19) **REPORT DOCUMENTATION PAGE**

READ INSTRUCTIONS BEFORE COMPLETING FORM

(18) 1. REPORT NUMBER: AFML-TR-76-146 (9) Final rept. 1 Apr 75 - 31 Mar 76

2. GOVT ACCESSION NO.

3. RECIPIENT'S CATALOG NUMBER

(6) 4. TITLE (and Subtitle): MEASUREMENT OF PROPERTIES AND RESPONSE FUNCTIONS OF LIQUID LUBRICANTS RELATED TO TRANSIENT VISCO-ELASTIC REGIMES.

5. TYPE OF REPORT & PERIOD COVERED: Final Report - 4/1/75 to 3/31/76

6. PERFORMING ORG. REPORT NUMBER

(10) 7. AUTHOR(s): Meyer H. Birnboim

(15) 8. CONTRACT OR GRANT NUMBER(s): F33615-75-C-5105 new

9. PERFORMING ORGANIZATION NAME AND ADDRESS
Rensselaer Polytechnic Institute
Department of Mechanical Engineering
Troy, New York 12181

10. PROGRAM ELEMENT, PROJECT, TASK AREA & WORK UNIT NUMBERS
Project # 73420306

11. CONTROLLING OFFICE NAME AND ADDRESS
Air Force Materials Laboratory
Air Force Systems Command
Wright-Patterson AFB, Ohio

(11) 12. REPORT DATE: 1 August 1976

13. NUMBER OF PAGES: 56

14. MONITORING AGENCY NAME & ADDRESS (if different from Controlling Office)

(12) 75p.

15. SECURITY CLASS. (of this report): Unclassified

15a. DECLASSIFICATION/DOWNGRADING SCHEDULE

16. DISTRIBUTION STATEMENT (of this Report)

Approved for public release; distribution unlimited.

(16) 7342 (17) 03

17. DISTRIBUTION STATEMENT (of the abstract entered in Block 20, if different from Report)

18. SUPPLEMENTARY NOTES

19. KEY WORDS (Continue on reverse side if necessary and identify by block number)

Lubrication
High Pressure
Viscoelastic
Light Scattering
Ultrasonic
Liquid/Glass

20. ABSTRACT (Continue on reverse side if necessary and identify by block number)

This report is concerned with measurements of the viscoelastic response functions over a wide range of frequency and pressure that are required for the mechanical characterization of lubricating oils. Both rheo-optical (light scattering) and mechanical (ultrasonic) methods are required to obtain the viscoelastic data. Several developmental aspects of the implementation of these techniques as well as some of the results are discussed herein. The emphasis

DD FORM 1 JAN 73 1473 EDITION OF 1 NOV 65 IS OBSOLETE S/N 0102-014-6601

UNCLASSIFIED

SECURITY CLASSIFICATION OF THIS PAGE (When Data Entered)

406357 VB

of this report is on (1) design considerations for an extended broad range light scattering photometer that includes Rayleigh line width measurements on the liquid, low frequency data analysis based on scattering from nonmagnetic and from magnetic spheres suspended in the liquid, and Brillouin line width measurements to yield both elastic modulus and loss of the liquids in the range circa $10^8$ - $10^9$ Hz, (2) design considerations and progress on the cross and on the diamond anvil high pressure light scattering cells and on pressure measurements are discussed, (3) experimental and analytical details of a new shear wave ultrasonic apparatus for the frequency range 2 - 40 MHz are presented along with calibration measurements on a variety of liquids. The particular significance of these measurements to polymer additives is discussed.

FOREWORD

This report was prepared by Rensselaer Polytechnic Institute, Troy, New York under USAF Contract No. F33615-75-C-5105. The contract was initiated under Project No. 7342, Task No. 734203. The work was administered under the direction of the Air Force Materials Laboratory, with Mr. Fred C. Brooks (AFML/MBT) acting as project engineer.

This report covers work conducted by the authors from 1 April 1975 to 15 March 1976. This report was submitted by the authors in March 1976.

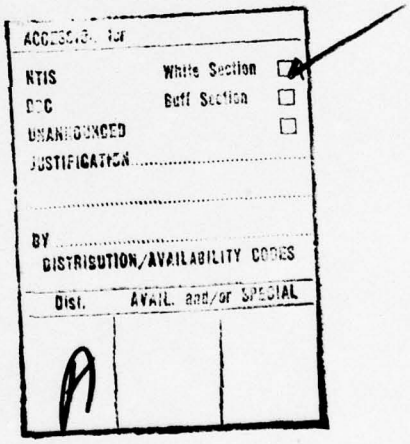

TABLE OF CONTENTS



PRECEDING PAGE BLANK-NOT FILMED

LIST OF ILLUSTRATIONS

## LIST OF SYMBOLS

| | |
|---|---|
| $\mu^*$ | Complex shear modulus (= $G^*$) (dynes/cm$^2$) |
| $\mu'$ | Shear storage modulus (= $G'$) (dynes/cm$^2$) |
| $\mu''$ | Shear loss modulus (= $G''$) (dynes/cm$^2$) |
| $\lambda$ | Lamé's constant (dynes/cm$^2$) |
| b | One-half thickness of delay line (cm) |
| SS(0) | Meitzler mode (or principal shear mode) |
| $\rho$ | Density (gm/cm$^3$) |
| $\varphi$ | Scalar potential |
| $\underset{\sim}{W}$ | Vector potential |
| $V_D$ | Dilatational wave velocity (cm/sec) |
| $V_S$ | Transverse wave velocity (cm/sec) |
| $\underset{\sim}{u}$ | Displacement vector (cm) |
| t | Time (sec) |
| $\omega$ | Angular frequency (radians/cm) |
| m | Complex propagation vector in z-direction |
| n | Complex propagation vector in x-direction |
| $\sigma$ | Stress ($\sigma_{xy}$ = shear stress) (dynes/cm$^2$) |
| I | Integer number |
| $Z^*$ | Mechanical impedance (dynes • sec/cm$^3$) |
| R | Mechanical resistance (dynes • sec/cm$^3$) |
| X | Mechanical reactance (dynes • sec/cm$^3$) |
| A | Attenuation constant (neper/cm) |
| B | Propagation constant (radians/cm) |
| $\Delta A$ | The difference of attenuation with and without liquid (neper/cm) |
| $\Delta B$ | The difference of phase shift with and without liquid (neper/cm) |
| $\lvert G \rvert$ | Magnitude of complex shear modulus (dynes/cm$^2$) |

LIST OF SYMBOLS (Cont'd.)

| | |
|---|---|
| $\eta^*(\omega)$ | Dynamic viscosity (dynes • sec/cm$^2$ or poise) |
| $\eta'(\omega)$ | Real part of dynamic viscosity (poise) |
| $\eta''(\omega)$ | Imaginary part of dynamic viscosity (poise) |
| $\overline{K}$ | Propagation constant (radians/cm) |
| A,C,D,E,F,H | Various constants |
| $K'$ | Bulk storage modulus |
| $K''$ | Bulk loss modulus |
| $\eta_v'(\omega)$ | Volume viscosity junction |
| $\tau$ | Relaxation time |
| $B'(\omega)$ | Bulk storage compliance |
| $B''(\omega)$ | Bulk loss compliance |
| f | Doolittle fractional free volume |

# SECTION I

# INTRODUCTION AND BACKGROUND

## A. FLUID PROPERTIES AND THE EHD LUBRICATION PROBLEM

In the elastohydrodynamic (EHD) lubrication problem the fluid undergoes a complicated stress/deformation history: the stresses are transient, and have both isotropic (pressure) and shear components. (See, for example, reviews by Dowson and Higginson [1] and Tallian [2].) The resultant compressional and shearing deformations must depend on the viscoelastic properties of the fluid, but in a rather complicated, and unknown way. One could pose the question: Given a particular stress history, what are the physical properties of the fluid which must be known in order to determine the resulting deformation history (or vice versa)?

Figure 1 illustrates the approach taken by Trachman [4]. The pressure distribution (peak pressure $p_o$) and geometry in the Hertzian contact zone (of width b) is indicated in this figure; the fluid undergoes a time varying pressure history as it flows through this contact region. By assuming a simple viscoelastic model for the liquid, and a specific pressure dependent viscosity function, the "effective" or "time dependent" viscosity for the liquid in the contact zone is calculated and shown in Figure 1b. By comparison, one sees that the "effective viscosity", hence shear traction, is much less than by assuming an equilibrium fluid with no relaxational part to the viscosity. Thus while one expects to enhance the viscosity, the transient contribution is less than the steady state value, therefore partially compensates. For such calculations however, a more complete knowledge of the shear and volume relaxational behavior of the liquids as well as appropriate time-pressure equivalence principles are required. One would expect that two liquids of different chemical character, although of the same atmospheric pressure steady state viscosity, would exhibit a dramatically different response in the contact zone. Thus, for practical as well as theoretical importance, a fuller understanding of the viscoelastic response is required.

## B. VISCOELASTIC PROPERTIES IN THERMODYNAMIC EQUILIBRIUM-PHENOMENOLOGICAL AND MOLECULAR DESCRIPTION

### 1. Behavior of the Linear Viscoelastic Parameters $\eta(\omega)$, $G'(\omega)$, $K'(\omega)$, $K''(\omega)$, $M'(\omega)$, $M''(\omega)$, $\tau_s$, $\tau_v$

In order to phenomenologically fully describe the mechanical response of a liquid in thermodynamic equilibrium at a pressure and temperature P,T we need the shear viscosity function $\eta_s(\omega)$, the shear modulus function $G'(\omega)$, the volume viscosity function $\eta_v(\omega)$ [or equivalent $K''(\omega)$ since $\omega\eta_v = K''(\omega)$], the bulk modulus function $K'(\omega)$. It is sometimes convenient to approximate these functions by their limiting values, and refer to a shear relaxation time $\tau_s$ and volume relaxation time $\tau_v(\tau \approx 1/\omega)$ at which a transition occurs between limiting values.

To develop a physical feeling for the useful parameters in describing material properties, it is convenient to collectively examine Figures 3 through 6. In Figure 3 (see Plazek [7]) the specific volume (reciprocal density) of the material is shown to vary with temperature; we shall allude to analogous variation with pressure. We ignore the possibility of crystallization. If we are in the "liquid" regime of this curve, and decrease the temperature slightly, then one expects the volume to decrease to its new equilibrium value "instantaneously"; certainly faster than our "time scale of measurement" $\tau$, for which we will assume $\tau$ = 1 second. Thus one could say that the structural relaxation $\tau_v$, is $\ll \tau$. The same would be true for an increment in pressure. By contrast, in the "glassy" regime of this curve, in response to a decrement in temperature (or increase in pressure) the volume would change very slowly. Thus the structural relaxation time $\tau_v$, the time for the sample to reach a new equilibrium volume is $\gg \tau$; indeed $\tau_v$ could be years. Hence notice that the glass temperature is not unique but depends on whether $\tau_v \gg \tau$ or $\tau_v \ll \tau$, namely depends on our choice for the time scale of the measurement.

Consider as an illustrative example of pressure dependence of the bulk dynamic compliance, $B^*(B^* = 1/K^*$, where $K^*$ is the bulk modulus), the reduced variable curve of Marvin [12], Figure 5b. The measurement time scale is taken as $\tau \sim 1/1000$ sec; at a reduced pressure $P_r$ = -2000 bars (or at high temperatures), $\tau_v \ll \tau$ and we obtain the liquid-like compliance $B_o$, whereas at a reduced pressure $P_r$ = +2000 bars, $\tau_v \gg \tau$ and then we obtain the glass-like compliance $B_\infty$. In these examples, the $\tau$ of the measurement is kept fixed and $\tau_v$ is changed by pressure or temperature! Alternatively, if the P and T are held constant as in Figure 5a and only $\tau$ is changed, then one measures a liquid-like compliance $B_e$ at $\tau \gg \tau_v$, and glass-like $B_g$ for $\tau \ll \tau_v$. This

figure illustrates that $\tau_v$ can be determined at each fixed T and P if $\tau$ is variable over a wide time (frequency) range. We now conclude that even the "liquid-like" regime of Figure 3 can behave "glass-like" if $\tau$ is short enough.

Hence the viscoelastic properties of the lubricant $B_e(P)$, $B_g(P)$ and $\tau_v(P)$ must be determined as a function of pressure. And more!

Turning next to the viscoelastic response of a lubricant to (dynamic) shear deformation, Figures 4a and b indicate additional parameters required to describe the fluid. There are two characteristic relaxation times* $\tau_c$ and $\tau_s$ if the lubricant contains polymers, through molecular models these are associated with conformational change of the polymers $\tau_c$, and orientational changes of the solvent molecules $\tau_s$. Thus, for $\tau \gg \tau_c > \tau_s$ (or $\omega \ll \omega_c < \omega_s$), the lubricant behaves liquid-like with a shear viscosity $\eta_0$ and "zero" shear modulus; for $\tau_c > \tau > \tau_s$, the viscosity drops to a new level of $\eta_\infty$ and the shear modulus G′ increases to rubber-like values; while for $\tau < \tau_s$ the viscosity drops further and G′ reaches a glass-like value.

Hence the shear viscoelastic properties of the lubricant $\eta_0(P)$, $\eta_\infty(P)$, $G_\infty(P)$, $\tau_c$ and $\tau_s$ must also be determined as a function of pressure.

As an aside, it should be mentioned that a polymeric fluid being sheared will also generate normal stresses which tend to push the contact surfaces apart. The magnitude of these normal stresses are related to $\eta_0$ and $\tau_c$.

## 2. The Free-Volume Picture: Concepts of Time-Temperature Superposition

One unifying model of liquids which has had a large degree of success in tying together temperature and pressure dependent properties has been the free volume model of Doolittle [8]. The idea is that the actual volume occupied by the molecules is less than the actual sample volume v, so that the difference is the free volume $v_f$. The larger the fractional free volume $f \equiv v_f/v$, the easier it is for molecules to slide past each other or to rearrange conformations. Thus Doolittle postulated that the temperature and pressure dependence of f would be linear:

$$f = f_0 + \alpha_f (T - T_0) + \beta_f (P - P_0) \qquad (1)$$

---

* In every case, by "characteristic relaxation time" we mean the mean value of the relaxation time distribution function.

and, further: that at two different temperatures T and $T_o$, each characteristic relaxation time would change in the same ratio as the zero shear viscosity, then a temperature shift factor is defined:

$$a_T \equiv \frac{\tau_\theta / \tau}{\tau_c / \tau_o} = \frac{\eta_o / \tau}{\eta_o / \tau_o} \tag{2}$$

from which he obtains

$$\ell n\, a_T = B\left(\frac{1}{f} - \frac{1}{f_o}\right) . \tag{3}$$

This equation was extended by Ferry [15] to the WLF equation

$$\ell n\, a_T = \frac{-C_1 (T - T_o)}{C_2 + T - T_o} \tag{4}$$

which, in combination with Eq.(2) has formed a time-temperature superposition principle that has been successful when applied to conformational relaxation times. The inference of such an equation is that the character of the relaxation mechanism does not change with temperature (pressure), but only the magnitude and characteristic time scale will change. This is not true for all relaxation mechanisms. The utility of a time-temperature superposition principle is that predictions can be extrapolated to time (or temperature) ranges other than those measured.

3. The Free-Volume Picture: Concepts of Time-Pressure Superposition

Time-pressure superposition is far less developed for large pressure ranges. Ferry [15] has extended the concepts above to obtain:

$$\log a_p = \frac{(B/2.303\ f_o)(P - P_o)}{f_o/\beta_f - (P - P_o)} . \tag{5}$$

The free-volume model would say that only the final volume is important regardless of the temperature or pressure history route. This idea needs further testing. Other approaches have been developed by Cohen [9] and by Gibbs [10].

C. VISCOELASTIC RESPONSE TO THE TRANSIENT (NONEQUILIBRIUM) EHD SITUATION

This subject of the relation of equilibrium properties to transient response has not thus far been studied extensively, and therefore is part of our experimental goals. One useful view taken by Harrison [11a] and by Trachman [4] utilizes free volume concepts discussed above. The central argument can be viewed

as if volume is the unifying concept, then pressure (and temperature) history may be put aside, and the response may be determined by integration over volume history, with the assumption of equilibrium properties at each segment of the history.

## D. EXPERIMENTAL TECHNIQUES

### 1. Mechanical Spectroscopy: Steady State, Low Frequency, Ultrasonic

The mechanical relaxation spectra of interest for lubrication liquids can reach from steady state (D.C.) to $10^{10}$ Hz. The part of the spectrum of interest will of course change for each pressure (and temperature). As indicated earlier the functions which must be known are the shear viscosity and modulus, and the bulk viscosity and modulus. While a variety of mechanical techniques extending from 1 Hz to $10^8$ Hz have been used in this laboratory (Figure 2) for liquids at atmospheric pressure, not all of them are directly applicable to high pressure techniques. Some exceptions are applications of similar methods to high pressure problems by Barlow [11], Marvin [12] and by Lamb [13].

The primary approach taken in our studies, is to construct a practical high pressure cell optimized so that the widest frequency range of measurements can be made in the same cell - both under equilibrium and transient pressures. Because of the limit of small sample volume, we emphasize the techniques which utilize light scattering, and those which couple mechanical viscoelastic techniques with light scattering - rheo-optic techniques.

### 2. Light Scattering - Twelve Years of Progress

With the advent of lasers, fast photomultipliers, highest quality Fabry-Perot interferometers, high speed (computerized) autocorrelators - material property information - extracted by light scattering has developed very far indeed these past twelve years. Here we will only list a few techniques relevant to lubrication, a few developed in our laboratory for the past eight years, many developed elsewhere.

The general features of the light scattering experiment is found in Figure 8. Light from a laser is focussed into a narrow beam (circa 0.1 mm) at the liquid sample, and the light scattered at any set scattering angle $\theta$ is collected by a photomultiplier. The "liquid" scattering cell may be one of the new high pressure cells of Figures 9 or 11, or our older high pressure cell (22)

of Appendix 1. The scanning photometer (26) paper provides a more detailed description. Optical detection can be direct as shown in Figure 8 for autocorrelation and cross-correlation function analysis of scattered intensity; or a Fabry-Perot Interferometer (FP) may be inserted between liquid and photomultiplier (PM) for Brillouin peak and Rayleigh Wing analysis; filters for fluorescence studies and analyzers for depolarized scattering are also introduced between liquid and PM.

(i) Rayleigh line. Figure 7 shows a light scattering spectrum from Benzene at $\theta = 90^{\circ}$ taken by Cummins [16] using a FP. The central line is called the Rayleigh line because the center frequency is the same as that of the laser. However, whereas the laser line width is a few Hz, this Rayleigh line is $\sim 10^{8}$ Hz and is due to nonpropagating entropy fluctuations, i.e., changes in local ordering of the molecules or rotational ordering of the molecules (when measured in HV). Notice VV refers to the polarized component of the light, HV to the depolarized component. Speed of molecular motion is related to line width.

(ii) Brillouin lines VV polarization. The lines on either side of the central line in Figure 7 are due to pressure fluctuations inherent in all materials; this becomes equivalent to an ultrasonically generated pressure disturbance which of course propagates as a wave. Such waves are spontaneously present at all frequencies (and wavelengths), so that one selects the acoustic wavelength by setting $\theta$, the scattering angle, and measures the frequency shift with respect to the central line to obtain the velocity. Together with the density of the fluid, this yields the longitudinal modulus M, where $M = K + \frac{4}{3} G$, see for example Dill [23] or McSkimin [24]. A more detailed discussion of the nuances in extracting K and G, as required for lubricant properties is omitted here. The width of these Brillouin peaks yields the wave attenuation, or dynamic viscosity $\eta_M$.

(iii) Brillouin lines HV polarization. If the frequency and pressure are such that the material behaves glass-like, and can sustain a shear stress, then a transverse velocity and attenuation corresponding to $G_\infty$ and $\eta_\infty$ can also be determined.

(iv) Quasi-elastic scattering. When polystyrene spheres of size $< \lambda_{light}$ are added in minute concentration to the liquid, they become the primary scattering source, and their relative motions give rise to time varying interference of

the light reaching the PM (no FP). The resulting photocount fluctuations are analyzed by the computer/autocorrelator as seen in Ref.26 and Appendix 1. The autocorrelation function yields diffusion coefficient of the spheres, hence one obtains the viscosity (low frequency limit) $\eta_0$ of the liquid.

(v) Quasi-elastic scattering. A new technique under development is to replace the polystyrene spheres used above with colloidal magnets and force mechanical oscillation at medium frequencies (1 Hz to 10 KHz) by an external magnetic field. The motion is analyzed by a cross-correlation technique related to the one used above.

## E. OBJECTIVES OF THIS RESEARCH PROGRAM

In elastohydrodynamic (EHD) lubrication the liquid lubricant is subjected to a complex transient stress history in which the isotropic pressure components may reach beyond 200,000 psi in durations of the order of 1 millisecond. One may ask: How do the viscoelastic characteristics of a fluid influence the stress built up in this lubrication situation: Therefore our long term objectives are:

(i) To measure the rheological properties of a variety of liquid lubricants over the full frequency range of viscoelastic response from 1 Hz to $10^{10}$ Hz; over a pressure range to 300,000 psi; and over a temperature range from -100°C to +300°C. Knowledge of the viscoelastic response is important both under equilibrium and transient pressure and temperature histories, as well as in uniform and nonuniform pressure/temperature fields.

(ii) Phenomenological theories are to be explored which can relate the above equilibrium state viscoelastic measurements to the stress/strain response of a liquid under transient elastohydrodynamic lubrication conditions. In other words, the studies should lead to time-temperature and time-pressure superposition principles applicable under transient and nonuniform conditions.

(iii) Molecular theories are to be examined which relate molecular structure to the measured macroscopic response; thereby establishing possible relations between lubricant properties and molecular structure.

(iv) Experimental procedures in this laboratory are based primarily on rheo-optic techniques; that is, application of stresses by external mechanical or by spontaneous means, and measurement of response by optical (laser light scattering) means.

(v) Selection of materials: After consultation with Mr. F.C. Brooks and Dr. J.F. Dill it was established that the fluid PR-143 AC would be most suitable for initial studies, and Emery 2958 and Stauffer 704 would be appropriate follow-on candidate fluids. In this discussion it was established that the most meaningful progress could be made if coordination between laboratories was established on the basis that each measured some identical fluids. Of course, an understanding of the relationship between chemical structure and mechanical properties of lubricants remains a continuing objective.

## SECTION II

## EXPERIMENTAL PROGRESS AND RESULTS

### A. THE LIGHT SCATTERING SPECTROMETER

Our light scattering spectrometer is in the process of being upgraded to add the capability of:

(i) Brillouin line width measurements for polarized and depolarized components.
(ii) Scattering from magnetic spheres in linear motion in the liquid.
(iii) Scattering from magnetic spheres in oscillatory motion in the liquid. These are additional to the capability hitherto available of:
(iv) Rayleigh (quasi-elastic) scattering.
(v) Scattering from suspended polystyrene spheres in Brownian motion.
In addition, for measurement of pressure, we must add the capability to measure:
(vi) Fluorescence spectral shift from ruby crystals.

A multiport microscope system has been designed to accommodate this variety of optical methods from the small volume of the high pressure cells. The major components of this new system have now been procured or were available from the previous system. It is useful to summarize the design considerations and present ststus of each of the major components of the light scattering spectrometer system.

#### 1. The Light Scattering Photometer

The restrictions imposed by a small volume high pressure cell (see discussion of cell), together with the requirement for several experiments have led us to the design of a multiport microscope light scattering photometer to replace our current apparatus. The microscope will have three ports as seen in Figure 12: one for direct visual or video scan observation of liquid to glass/crystalline transformations (and kinetics thereof) under high pressure; one port for quasi-elastic light scattering (Rayleigh line) data analysis including oscillating magnetic spheres and for Brillouin and Rayleigh wing spectral analysis; and one for determining local pressure by the fluorescent spectral shift of ruby as measured with an optical scan spectrometer.

For the diamond anvil high pressure cell, surface scattering can be a serious problem. In our previous experience with scattering from capillary tube cells, we were able to first keep the surface scattering localized by adjustment of the angle between the cell and incident beam, and then adjustment of the angle and volume of observation so that the surface regions were excluded from view. Since a (estimated) $\pm$ 20° rotation of optical access to the cell is possible, we must provide for these angular adjustments to minimize the amount of surface (liquid-diamond interface) scattered light that enters the optical system.

To accommodate the remaining surface effects: (a) For autocorrelation the surface will act as a reference signal (i.e., no frequency shift), therefore the method will become hetrodyne instead of homodyne; (b) for Brillouin scattering the unshifted line can be tuned (with our new laser - see below) to an Iodine ($I_2$) absorption band. This means the $I_2$ acts as a sharp band reject filter of width 900 MHz; (c) for fluorescence the additional scattering is less important. The air suspended granite optical table remains excellent for the new system. New mounting fixtures will be required for the new laser, Fabry-Perot, multiport microscope and goniometer.

2. The Argon Laser

One of the major new components is the Argon Laser to replace our present HeNe laser. For Brillouin line width measurements, particularly at small scattering angles and where correlation techniques and the Fabry-Perot interferometer techniques can overlap, it is essential that the laser source be as stable (in frequency) as possible. Amplitude stability is required for the quasi-elastic (intensity fluctuation) experiments. Towards this end, the following test for amplitude and frequency stability was devised.

The laser etalon was first adjusted so that the single frequency of the laser corresponds to the absorption peak in an Iodine absorption cell and the intensity $I_p$ is monitored on an oscilloscope. Then the etalon is then adjusted to the shoulder of the Iodine absorption and the intensity $I_s$ is monitored. The percentage fluctuations in $I_p$ are due to amplitude noise, while fluctuations in $I_s$ contain both amplitude and frequency noise. The spacing between longitudinal modes of the laser were used for frequency calibration.

The two commercially available argon lasers considered most stable, Spectra Physics Model 165 and Lexel Model 85, were tested in this way. On the basis of performance, the Lexel laser was found preferable.

A more powerful version of the Lexel 85, the Lexel 95, was finally selected and has been delivered. We are attempting to pre-chill the laser cooling water to achieve laminar flow of the coolant, since acoustic noise generated by turbulent flow is partially responsible for the noise in the laser frequency spectrum.

3. The Fabry-Perot Interferometer

Another major component is the Fabry-Perot interferometer for Brillouin shift and line width measurements. After comparison of specifications of Tropel and Burleigh units, the Burleigh Fabry-Perot Interferometer Model RC10 with multipass option was selected. Aside from stability, we concluded that the multipass feature of this unit will be very helpful in the reduction of the contribution of scattering from the surfaces of the diamond cell. Agreement was reached with RPI for the purchase of this unit, and the unit has been delivered.

The unit is being set up and interfaced to the computer. The electronics for individual adjustment of the three piezoelectric drivers and the high voltage sweep circuit must still be constructed and interfaced to the digital to analog drives from the computer (Figure 10). Also the computer program for tuning the interferometer and for automatic frequency drift correction must still be written.

4. Photodetection

The photodetection system based on our present thermoelectrically cooled Amperex 56 TVP photomultiplier will be adequate for the present; a lower background ITT FW130 phototube may be desirable at a later stage. An adapter to mechanically couple this phototube housing to the collimator collection optics of the Fabry-Perot must be constructed.

5. Data Acquisition System

The present computerized data acquisition and analysis (autocorrelation) system as seen in Figure 12, continues to work well. Only more software will be required for the new functions.

No additional hardware is required. The same software auto- and cross-correlation programs will be used, and only an automatic sweep normalization program has to be written for the new Fabry-Perot.

6. Other Considerations

Several of the components of our earlier light scattering system are being incorporated in the new Diamond Cell Light Scattering geometry. We are still in the process of assembly, so that some minor components must still be selected, and several mounting fixtures must be constructed in the workshop.

For the high pressure dynamic viscosimeter method, magnetic spheres are suspended in the lubricant in the diamond cell, and these are oscillated by an external magnetic field.

We have explored a variety of colloidal magnetic particles and tiny iron spheres for use in the high pressure cell dynamic viscosity technique. The colloidal suspensions compatible with the lubricants to be studied have shown a tendency to aggregate. The tiny iron spheres seem to work well in the lubricants. These were available from Whittaker Corporation in 250 $\mu$ and 50 $\mu$ diameters, suitable for our experiments. They can be individually handled. We are testing a variety of magnetic field drive geometries.

B. HIGH PRESSURE CELLS

We have decided to pursue two high pressure cell designs in this laboratory, the cross cell and the diamond anvil cell.

1. The Cross Cell Design

Earlier measurements [22] on light scattering from suspended spheres were made in this laboratory (Appendix A) over the pressure range up to 35,000 psi. The cell worked well, but the range is less than pressures generated in the EHD regime, so a new cross cell of similar design was proposed to extend the range beyond 150,000 psi. In this modified design (Figure 9), the sample volume was substantially reduced so that pressure transmission would not be impeded by the transition of the sample from liquid-like to glass-like behavior, and so that the same valve stem would serve as the compression piston. The latter would then permit transient pressure pulses to be applied.

The major advantage of this cross cell design is that scattering can be observed at 90° thereby eliminating the surface scattering contribution. The disadvantage is that material failure limits the highest achievable pressures.

2. Diamond Anvil Cell

The basic design of the reho-optic light scattering high pressure cell instrument is centered on microscopic observation of the fluid under high pressure. The use of a tiny volume as in the diamond cell (see Figure 11) seems essential if one is to achieve pressures in the 300,000 psi range, since the transition from liquid-like to glass-like behavior of the sample would resist the pressure build-up. Furthermore, the cell volume becomes orders of magnitude closer to the volume in EHD contacts, so that one brings the laboratory experiment much closer to the real contact situation. The process of generating high pressures (and impulses) becomes simplified, a single hand screw is sufficient to generate the desired pressures. The additional complexities that arise from the microscopic volume are connected with sample loading, measurement of pressure, and surface scattering. Furthermore, microscope optics are required for the small sample volume, and were described above.

A diamond anvil cell designed by Dr. A. Van Valkenberg, while at the National Bureau of Standards, was ordered and delivered from High Pressure Diamond Optics, Incorporated. Both optical and sample handling procedures are currently being developed for these samples of volume circa $10^{-4}$ cc.

Pressure and pressure distribution measurement can be determined by the shift in the fluorescence spectra of ruby crystals suspended in the fluid [18, 19] and locally monitored by the microscope optics. Design is underway for the fast pressure pulse triggering device.

C. ULTRASONIC SHEAR WAVE APPARATUS

1. Introduction and Preliminary Results

There are several atmospheric pressure reference state measurements that are required for proper interpretation of higher pressure data. One of the more important is the high frequency limiting shear viscosity and modulus (transverse wave) and relaxation time(s). Steady-state shear viscosity (low frequency limit) data is available for the test fluids, however, the directly measured high frequency limiting shear modulus appears to be lacking. Since Brillouin scattering

from shear waves is difficult to observe, the high frequency limit $G'_\infty$ and $\eta'_\infty$ must be calculated from the longitudinal modulus with some assumptions. Therefore, we assembled auxiliary ultrasonic delay line apparatus for direct measurement of $G'$ and $\eta'$ even though it is only useful at 1 atmospheric pressure. This apparatus is currently being calibrated in the frequency range 2 to 50 MHZ and over a temperature range from -10°C to +70°C. Thus this apparatus serves two purposes: (i) to provide the high frequency shear moduli and relaxation times mentioned above for bulk lubricants and (ii) to provide the limiting shear relaxational behavior for lubricants with polymer additives (i.e., a measure of the configurational relaxation contribution of the polymer additive).

This apparatus has been constructed, tested, calibrated, and we are now in the process of measuring Krytox 143.

Calibration curves have been obtained for several fluids which we believe to be Newtonian up through the frequencies of interest.

Preliminary results have also been obtained on solutions of polystyrene in a di-2-ethyl-hexyl phthalate fluid. These results are relevant to the role of polymer additives; and indicate that at high frequencies the viscosity of the solution does not become that of the solvent. Namely, theory has assumed that when conformational relaxation of the polymer has been "frozen out", then only the viscosity of the solvent would remain. This picture is incomplete. More extensive data and analysis of this phenomenon, called the $\eta_\infty$ problem, is in progress.

2. Description of Apparatus

The description of this apparatus may be found in Appendix B, coupled with Figures 10 and 13. The derivation of basic device equations follow.

## 3. Derivation of Basic Surface Wave Loading Equations for Delay Line

In this experiment the main interest is measuring the complex shear modulus $\mu^*$ of the liquid sample which is in contact with major surfaces of the delay line. The equations for propagation of ultrasonic waves in a plate are developed in this section and then restricted to the case of interest, namely, the lowest order transverse mode. This mode is often called the Meitzler mode [1]. We obtain solutions for the velocity and attenuation of this wave in the presence and absence of liquid at the interface. Equations for the relationship between velocity and attenuation change and the mechanical impedance and the shear modulus of the liquid are also obtained.

Consider an infinite plate (Figure 13) of thickness 2b in a coordinate system, where it is bounded by the major planes at X = b and X = -b with a liquid sample. When an ultrasonic transverse wave propagates down the plate in the z-direction a wave is also generated in the liquid because of the no-slip condition between solid plate and liquid at the interface.

The steady-state sinusoidal excitation with the appropriate boundary conditions results in a set of homogeneous equations whose solutions have discrete modes of wave propagation.

For the delay line used here, the dimensions and polarization of the piezoelectric (P.Z.T. ceramic transducer material) are chosen so that only the principal shear mode (Meitzler mode) of propagation is excited while higher shear modes are suppressed (when the plate is in vacuum). It is very useful to have only the nondispersive Meitzler mode SS(0) because its velocity is independent of frequency and the complication of having several modes of different velocities can be avoided.

Even in the presence of liquid on the major surfaces it will be assumed that only the same SS(0) mode is present since the mechanical impedance of the liquid is much less than the solid.

The equation of wave propagation for an isotropic homogeneous linear viscoelastic material is generally written as follows:

$$\mu^*\nabla^2\underset{\sim}{u} + (\lambda+\mu^*)\ \underset{\sim}{\nabla}(\underset{\sim}{\nabla}\cdot\underset{\sim}{u}) = \rho\frac{\partial^2 u}{\partial t^2}, \qquad (1)$$

where

$\mu^*$ - complex shear modulus

$\lambda$ - other Lamé coefficient

$\underset{\sim}{u}$ - particle displacement vector

$\rho$ - density.

If one uses Hamilton's decomposition method by defining

$$\underset{\sim}{u} = \nabla\varphi + (\underset{\sim}{\nabla} \times \underset{\sim}{W}) \tag{2}$$

in terms of scalar and vector potentials $\varphi$ and $\underset{\sim}{W}$, then the following wave equations in $\varphi$ and $\underset{\sim}{W}$ are obtained from (1):

$$V_D^2 \nabla^2 \varphi = \frac{\partial^2 \varphi}{\partial t^2} \tag{3}$$

$$V_S^2 \nabla^2 \underset{\sim}{W} = \frac{\partial^2 \underset{\sim}{W}}{\partial t^2} \tag{4}$$

with

$$\underset{\sim}{\nabla} \cdot \underset{\sim}{W} = 0 \tag{5}$$

where

$$V_S = \sqrt{\frac{\mu^*}{\rho}}$$

$$V_D = \sqrt{\frac{2\mu^* + \lambda}{\rho}}$$

in which $V_S$ and $V_D$ are the transverse and dilatational wave velocities.

In our delay line device, the transducers are polarized to provide displacements with a component in the y-direction only, hence we assume $u_x = u_z = 0$. Thus the wave had displacement $u_y = u_y(x,0,z,t)$ in the y-direction only; the displacement is assumed to be the same everywhere in y. Thus Eqs.(3) and (4) reduce to:

$$\mu^* \nabla^2 u_y = \rho \frac{\partial^2 u_y}{\partial t^2} \tag{6}$$

and

$$\mu^* \left( \frac{\partial^2 u_y}{\partial x^2} + \frac{\partial^2 u_y}{\partial z^2} \right) = \rho \frac{\partial^2 u_y}{\partial t^2} \ . \tag{7}$$

Equation (7) is a shear wave equation with complex shear modulus $\mu^*$ (one of Lamé's constants). By the application of the method of separation of variables to Eq.(7), namely $u_y(x,0,z,t) = u_y(x,0,z)e^{i\omega t}$, one obtains for the

total solution of Eq.(7)

$$u_y = Ae^{i\omega t}(Ce^{mz} + De^{-mz})(Ee^{nx} + Fe^{-nx}) \tag{8}$$

where $\omega$ is the angular frequency, A,C,D,E,F are constants to be determined by the boundary conditions, and m and n are the complex propagation constants in the z- and x-directions, respectively.

Displacement Boundary Conditions

This same equation can now be applied to each of the three regions of interest: the solid delay line and the upper and lower liquid layers; then the boundary conditions are matched. In steady state the frequencies are the same in all regions.

Consider the transverse wave in the viscoelastic medium above and below the plates. This wave is traveling unbounded in the positive z- and x-directions and since it is traveling in an attenuating medium, the displacement must approach zero as z and x approach infinity. Then C = E = 0 in the liquid above the plate and similarly C = F = 0 in the liquid below the plate.

In the plate itself the waves are bounded in the x-direction and thus there is only one boundary condition that is C = 0. The solutions can be obtained as follows:

$$u_{y_0} = H_0 e^{-m_0 z} e^{-n_0 x} e^{i\omega t} \tag{9a}$$

$$u_{y_1} = H_1 e^{-m_1 z} e^{i\omega t}(e^{n_1 x} + e^{-n_1 x}) \tag{9b}$$

$$u_{y_2} = H_0 e^{-m_0 z} e^{n_0 x} e^{i\omega t} \tag{9c}$$

where the subscripts 0, 1, 2 designate the region above the plate, the region within the plate and the region below the plate, respectively. The symbols $H_0$ and $H_1$ are appropriate combinations of A,C,D,E,F.

Stress Boundary Conditions

In the presence of liquid the stress continuity across the plane boundary, $x = \pm b$, requires that:

$$\sigma_{xx} \approx 0 \tag{10a}$$

$$\sigma_{xy} = \mu^* \frac{\partial u_y}{\partial x} \tag{10b}$$

$$\sigma_{xz} = 0. \tag{10c}$$

If the plate is in vacuum, all component stresses across the plate surface must be zero, hence from $\sigma_{xy} = \mu^* \frac{\partial u_y}{\partial x} = 0$ at $x = \pm b$ one obtains

$$e^{n_1 b} = e^{-n_1 b} . \tag{11}$$

Thus real $[n_1] = 0$ and

$$IM[n_1] = \frac{\pi I}{b} , \quad I = 0, 1, 2, \ldots . \tag{12}$$

If we now restrict our consideration to the solution with I = 0 (the Meitzler mode), Eq.(9) for the wave in the plate becomes

$$u_{y_1} = 2H_1 e^{-m_{1V} z} e^{i\omega t} \tag{13}$$

where $m_{1V}$ and $m_{1L}$ will refer to the propagation vector in the solid, in the z-direction, in the absence and presence of liquid.

If the plate is in a viscoelastic liquid, the complex shear modulus of the liquid $\mu^*$ is obtained from the stress continuity equation (10b) combined with Eq.(9b) to yield:

$$\mu_o^* = \mu_1 \frac{n_1 (1 - e^{2 n_1 b})}{n_o (1 + e^{2 n_1 b})} \tag{14}$$

since $(\sigma_{xy})_o = (\sigma_{xy})_1$, at $x = b$.

Next, the following wave vector relation for the liquid is obtained from Eqs.(9a) and (7):

$$m_o^2 + n_o^2 + \frac{\omega^2 \rho_o}{\mu_o^*} = 0 . \tag{15}$$

From displacement continuity across the plate, $u_{y_o} = u_{y_1}$ at $x = +b$ for all values of z. Thus by equating Eqs.(9a) and (9b), one concludes that

$$m_o = m_{1L} . \tag{16}$$

Hence Eq.(15) can be combined with (16) to obtain an equation that couples wave vectors in the liquid and in the solid:

$$m_{1L}^2 + n_o^2 + \frac{\omega^2 \rho_o}{\mu_o^*} = 0 . \tag{17}$$

Next, the following wave vector relation for the plate (in liquid contact) is obtained from Eqs.(9b) and (7)

$$m_{1L}^2 + n_1^2 + \frac{\omega^2 \rho_1}{\mu_1} = 0 \ . \tag{18}$$

While for the plate in vacuum, we have shown by Eq.(12) that $n_1 = 0$ for the Meitzler mode, thus the wave vector relation (18) becomes

$$m_{1V}^2 + \frac{\omega^2 \rho_1}{\mu_1} = 0 \ . \tag{19}$$

In our experiment $m_1$ is measured in air (i.e., vacuum) and again in liquid. Thus by combining Eqs.(18) and (19) we obtain

$$m_{1L}^2 - m_{1V}^2 = - n_1^2 \ . \tag{20}$$

The complex modulus of the viscoelastic liquid $\mu_0^*$ can be obtained by using the experimental values of Eq.(20) together with Eqs.(14) and (17) to give a quadratic equation for $\mu_0^*$. Alternatively, an explicit relation to the mechanical impedance of the liquid $Z^*$, can be obtained as seen below.

Notice some assumptions that were made in the preceding discussion: (1) Motions are steady-state sinusoidal of small amplitude so that nonlinear response of the propagating media can be neglected; (2) the plate is assumed to be isotropic and homogeneous and (3) the transducer will only excite the non-dispersive SS(0) mode.

## Relation of Mechanical Impedance of Liquid to Propagation Vector in Solid

The equations derived in the preceding section can also be related to the mechanical impedance $Z_0^*$ of the liquid.

*The mechanical impedance of a material is defined as the ratio of the stress to the particle velocity produced by that stress at any surface through the material.* For the shear stress components of interest here in the liquid we can write

$$Z_0^* \quad \frac{\sigma_{xy_0}}{\dot{u}_{y_0}} \tag{21a}$$

or

$$\sigma_{xy_0} = Z^* \dot{u}_{y_0} \ . \tag{21b}$$

It can be shown that the characteristic (shear) mechanical impedance for an unbounded liquid is related to the complex shear modulus and density by

$$Z_o^* = (\rho_o \mu_o^*)^{\frac{1}{2}} \quad . \tag{22}$$

Across the liquid-plate interface, $x = +b$, we have seen that displacement and stress must be continuous, hence velocity and stress/velocity must also be continuous.

At $x = b$

$$u_{y1} = u_{yo} \tag{23a}$$

$$\dot{u}_{y1} = \dot{u}_{yo} \tag{23b}$$

$$\sigma_{xy1} = \sigma_{xyo} = Z_o^* \dot{u}_{yo} \tag{23c}$$

and

$$\frac{\sigma_{xy1}}{\dot{u}_{y1}} = \frac{\sigma_{xyo}}{\dot{u}_{yo}} = Z_o^* \quad . \tag{23d}$$

Since we had for displacement and stress in the plate

$$u_{y1} = 2H_1 \cosh n_1 x e^{-m_1 z} e^{i\omega t} \tag{24}$$

$$\sigma_{xy1} = 2H_1 \mu_1 n_1 \sinh n_1 x e^{-m_1 z} e^{i\omega t} \quad , \tag{25}$$

the values of these functions at $x = b$ are substituted into Eq.(23d) to obtain

$$Z_o^* = -i \frac{\mu_1 n_1}{\omega} \tanh n_1 b \quad . \tag{26}$$

If we expand $\tanh n_1 b$, and take $|n_1 b| \ll 1$,

$$\tanh n_1 b = n_1 b + \frac{(n_1 b)^3}{3} + \ldots . \tag{27}$$

then

$$\boxed{Z_o^* = i \frac{\mu_1 n_1^2 b}{\omega}} \tag{28}$$

We had Eq.(20), that is,

$$-n_1^2 = m_{1L}^2 - m_{1V}^2 \quad . \tag{20}$$

It is convenient to write the complex propagation constants in their component form:

$$m_{1V} \equiv A_o + iB_o \tag{29a}$$

and

$$m_{1L} \cong A + iB \tag{29b}$$

where $A_o$, $B_o$ and A, B are the attenuation and propagation constants in the plate in the absence and presence of liquid, respectively. Hence, from Eq.(20):

$$-m_1^2 = (A + iB) - (A_o + iB_o)^2 \ . \tag{30}$$

For the usual case* where

$$(B + B_o) \gg (A + A_o) \tag{31}$$

Eq.(30) becomes

$$-n_1^2 = 2B_o(-\Delta B + i\Delta A) \tag{32}$$

where

$$\Delta A = A - A_o \text{ and } \Delta B = B - B_o \tag{33}$$

and from Eqs.(19) and (29a)

$$B_o = \left(\frac{\rho_1 \omega^2}{\mu_1}\right)^{\frac{1}{2}} \ . \tag{34}$$

Now Eq.(28) is rewritten as:

$$\boxed{Z_o^* = 2V_s \rho_1 b(\Delta A + i\Delta B)} \tag{35}$$

This is the basic experimental equation that relates the mechanical impedance of the liquid to the measured differences in attenuation and phase in the plate delay line.

---

* Assume $B_o \approx B$, and from Eqs.(31),

$$\begin{aligned}(A + iB)^2 - (A_o + iB_o)^2 &= A^2 - A_o^2 - B^2 + B_o^2 + 2i(AB - A_oB_o) \\ &= (A - A_o)(A + A_o) - (B - B_o)(B + B_o) + 2i(AB - A_oB_o) \\ &= (B + B_o)\left(\Delta A \frac{A + A_o}{B + B_o} - \Delta B + 2i \frac{\Delta A \cdot B_o}{B + B_o}\right) \\ &= 2B_o(-\Delta B + i\Delta A) \ .\end{aligned}$$

It is convenient to summarize the interrelation between the mechanical impedance and the complex shear modulus parameters for description of the liquid. These relationships are based on the linear theory of viscoelasticity. Also note that in viscoelastic convention, the symbol $G^* \equiv \mu^*$ for the shear modulus:

$$Z^* \equiv R + iX \tag{36}$$

$$G^* \equiv G' + iG'' \tag{37}$$

$$|G| \equiv (G'^2 + G''^2)^{\frac{1}{2}} \tag{38}$$

$$Z^* = (\rho_o G^*)^{\frac{1}{2}} \tag{39}$$

$$R = \rho_o^{\frac{1}{2}}(|G| - G')^{\frac{1}{2}} \tag{40}$$

$$X = \rho_o^{\frac{1}{2}}(|G| - G')^{\frac{1}{2}} \tag{41}$$

$$G' = (R^2 - X^2)/\rho_o \tag{42}$$

$$G'' = 2RX/\rho_o \tag{43}$$

$$G^* = i\omega\eta^* \tag{44}$$

$$\eta^* \equiv \eta' - i\eta'' \tag{45}$$

where R and X are mechanical resistance and reactance, $\rho_o$ the liquid density, $G'$ and $G''$ are the shear storage and loss moduli, $\eta'$ and $\eta''$ are the real and imaginary components of dynamic viscosity.

## D. CAPILLARY TUBE VISCOMETRY AND PICNOMETRY

The steady-state viscosity and density of the test fluids at atmospheric pressure is required for analysis of the ultrasonic data. The following tables summarize the measured values. The corresponding ultrasonic data are to be measured shortly.

Fluid: MLO-71-6

Composition: Perfluoroalkyl polyether

Pressure: 1 Atmosphere

| Temperature °C | Viscosity (Poises) | Density g/cc |
|---|---|---|
| 25° | 11.96 | 1.89 |
| 20° | 16.60 | 1.90 |
| 15° | 23.53 | 1.90 |
| 10° | 34.47 | 1.91 |
| * 25.0 | 11.43 | 1.90 |
| * 37.8 | 5.33 | 1.88 |
| * 98.9 | .488 | 1.78 |
| * 148.9 | .160 | 1.69 |

* This data has been supplied by Mr. F.C. Brooks of the Air Force Materials Laboratory, but not on the identical sample.

Fluid: ATL-5066
(Emery 2958)

Composition: Di-2-ethylhexyl azelate

Pressure: 1 Atmosphere

| Temperature °C | Viscosity (Poises) | Density g/cc |
|---|---|---|
| 25° | .156 | 0.908 |
| 20° | .189 | 0.911 |
| 15° | .232 | 0.915 |
| 10° | .287 | 0.918 |

Fluid: ATL-5067
(Stauffer 704)

Composition: Tri-methylol propane triheptanoate

Pressure: 1 Atmosphere

| Temperature °C | Viscosity (Poises) | Density g/cc |
|---|---|---|
| 25° | .239 | .958 |
| 20° | .286 | .959 |
| 15° | .355 | .962 |
| 10° | .449 | .963 |

## SECTION III

## CONCLUSIONS

We have been proceeding rather cautiously in trying to achieve both the short and long term objectives, and trying to test each step along the way. But we do feel that the development of the Diamond Cell Light Scattering Apparatus will provide an optimum and unique facility whereby extensive data about the phenomenological and molecular properties of the lubricant can be obtained under laboratory conditions that come closest to stimulation of actual EHD bearing lubrication.

# APPENDIX A

## A NOVEL METHOD FOR VISCOSITY MEASUREMENTS AT HIGH PRESSURES

Meyer H. Birnboim and H. Weiss
Mechanics Division
Rensselaer Polytechnic Institute
Troy, New York 12181

# A NOVEL METHOD FOR VISCOSITY MEASUREMENTS AT HIGH PRESSURES

The technique of quasi-elastic light scattering is utilized as a method to determine the viscosity of fluids subjected to large hydrostatic pressures. In this method, a small concentration of insoluble polystyrene spheres of known diameter, 0.109 microns, were added to the fluid, water. The high pressure cell in which the fluid is contained has three optical windows. The laser light scattered from the suspended spheres is analyzed to determine the diffusion coefficient of the spheres. Since, by Stokes law,

$$\eta = \frac{kT}{8\pi rD} \tag{1}$$

the viscosity of the fluid is determined from the measured diffusion coefficient and known particle radius r. A small correction is required for the contraction of the sphere and for refractive index change of the water under pressure. Results on the viscosity of water at 25°C up to pressures of 2.5 kilobars is reported and compared to published results.

The high pressure system and scattering cell (1) is illustrated in Figure 1. The system is assembled from standard* high pressure components. The scattering cell consists of a high pressure cross; three blank conical plugs are drilled out and fitted with sapphire cylinder windows which are epoxied in place. Windows from 1/8" to 1/4" diameter by 3/4" long have been used successfully to pressures of 35,000 psi. The fluid is filled through the reservoir to overflow at the window to ensure that no air is trapped, then the window plug is tightened. Pressure is generated by hand, by compression

---

* American Instrument Company, Silver Springs, Maryland.

of fluid in the valves. The sequence is: close all valves, open valves A, B, close A, open C, close B, C, then repeat sequence from open valves A, B. Three repetitions of the sequence will bring the pressure to 35,000 psi for a water sample.

The light scattered by the polystyrene spheres is observed at a scattering angle of 90° to the main beam. The intensity of scattered light is monitored by a photomultiplier which is operated in a photon counting mode, thus the number of photoelectric events (photocounts) per second n(t) is proportional to the intensity of light. The intensity is not constant on short time scales but exhibits fluctuation associated with the Brownian motion of the scattering particles [see review by Cummins and Swinney (2)]. The sequence of "instantaneous" intensities are stored in real time in the memory of a computer, then the autocorrelation function is calculated.

The photocount rate autocorrelation function $c(\tau)$ is defined in terms of the sequence n(t); and in turn $c(\tau)$ is related (2) to the translational diffusion coefficient D:

$$c(\tau) \equiv \langle n(t)n(t+\tau)\rangle_t = \langle n(t)\rangle\, \delta(\tau) + \langle n(t)\rangle_t^2 + Ae^{-2DK^2\tau} \qquad (2)$$

The brackets $\langle\ \rangle_t$ denote the average overall starting times t; $\delta(\tau) = 1$ for $\tau = 0$ and $\delta(\tau) = 0$ otherwise.

For our computer method, the real time t and delay time $\tau$ are always a multiple of T, that is $t = jT$ with $j = 0,1,2 \ldots$ ; A is a coefficient related to the intensity of light scattered from the macromolecules; and the magnitude of the scattering vector $\vec{K}$ is obtained from

$$K^2 = \left(\frac{4\pi n_o}{\lambda_o}\right)^2 \sin^2\frac{\theta}{2} \qquad (3)$$

where $n_o$ and $\lambda_o$ are the refractive index of the solution and wavelength of the light in vacuum. In this experiment, the scattering angle $\theta$ was kept at $90^\circ$. The correlation time, $1/2\ DK^2$, and therefore D, is calculated from the slope of $\ell n\left[c(\tau) - \langle n(t)\rangle^2\right]$ vs. $\tau$, where the shot noise, the first term of Eq.(2) may be neglected since it is zero except at $\tau = 0$, and $\langle n(t)\rangle_t$ is the average count rate.

An example of the autocorrelation function is seen in Figure 2, taken at a pressure of 15,000 psi. The diffusion coefficient determined from the slope of this curve in conjunction with Eq.(1) yields the viscosity at 15,000 psi. Our results for the limited pressure range of 0 to 35,000 psi (2.5 kilobars) taken at a temperature of $23^\circ$C are shown by the points in Fig.3. These points are superposed on the extensive data of Butt and Capi (3) as represented by the solid lines. The results are only intended as an illustrative example of the method.

Meyer H. Birnboim
H. Weiss
Rensselaer Polytechnic Institute
Troy, New York 12181

Acknowledgement

The authors gratefully acknowledge the valuable suggestions of Mr. W. E. Hake of American Instrument Company, Inc. in the design of the high pressure cell. This work was supported by a Research Grant GB 8770 from the National Science Foundation.

References

1. Bridgman, P. W., Proc. Amer. Acad. Sci., 61, 57 (1926).

2. Cummins, H. Z. and Swinney, H. L. in "Progress in Optics," ed. E. Wolf, North Holland Publishing Company, pp. 135-200 (1970).

3. Bett, K. E. and Cappi, J. B., Nature, 207, 620 (1965).

## FIGURE CAPTIONS

Figure 1 — Block diagram of the Homodyne Spectrometer and high pressure cell for the quasi-elastic light scattering experiment. Light scattered at an angle of 90° is detected by the photomultiplier. The number of photoelastic pulses $n_i$ in each successive interval of length T are stored in the memory of the computer.

Figure 2 — Plot of $\ln [ \langle n_i n_{i+j} \rangle_i - \langle n_i \rangle_i^2 ]$ vs. delay time $\tau_j$ at a scattering angle of 90° and atmospheric pressure. The photopulse autocorrelation function $\langle n_i n_{i+j} \rangle_i$ and the average number of counts are calculated from the measured sequence $n_i$. The $\tau_j = jT$, where $j = 0,1,2,\ldots$ . As discussed in the text, the slope of the above curve yields $\tau_c^{-1} \cong 2D_\pi K^2$, where $\tau_c$ is the characteristic correlation time.

Figure 3 — Viscosity of water vs. pressure. The filled points and solid lines are data of Bett and Cappi. The open circles and dashed lines are our data.

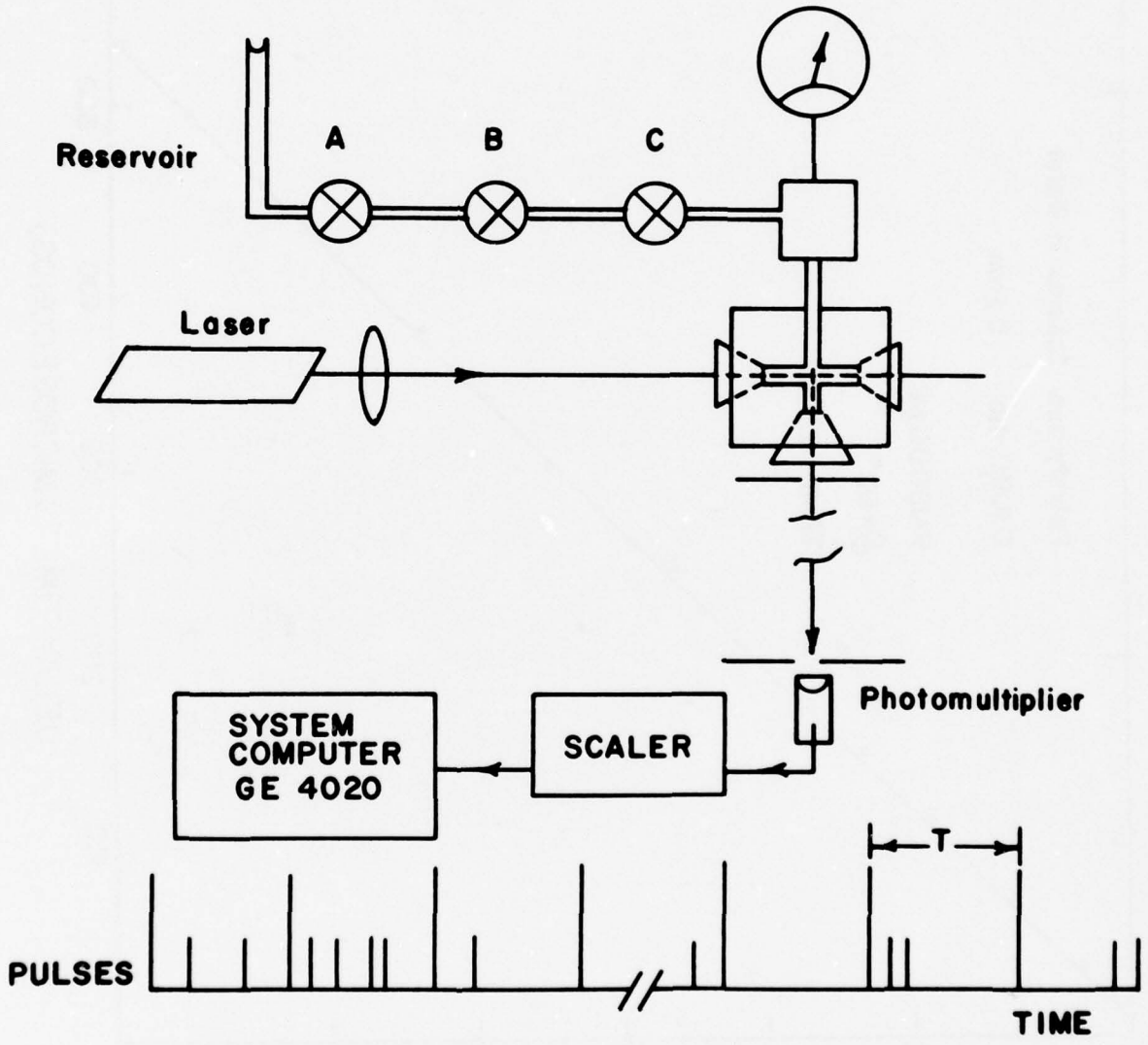


Figure 1 Block Diagram of the Homodyne Spectrometer.

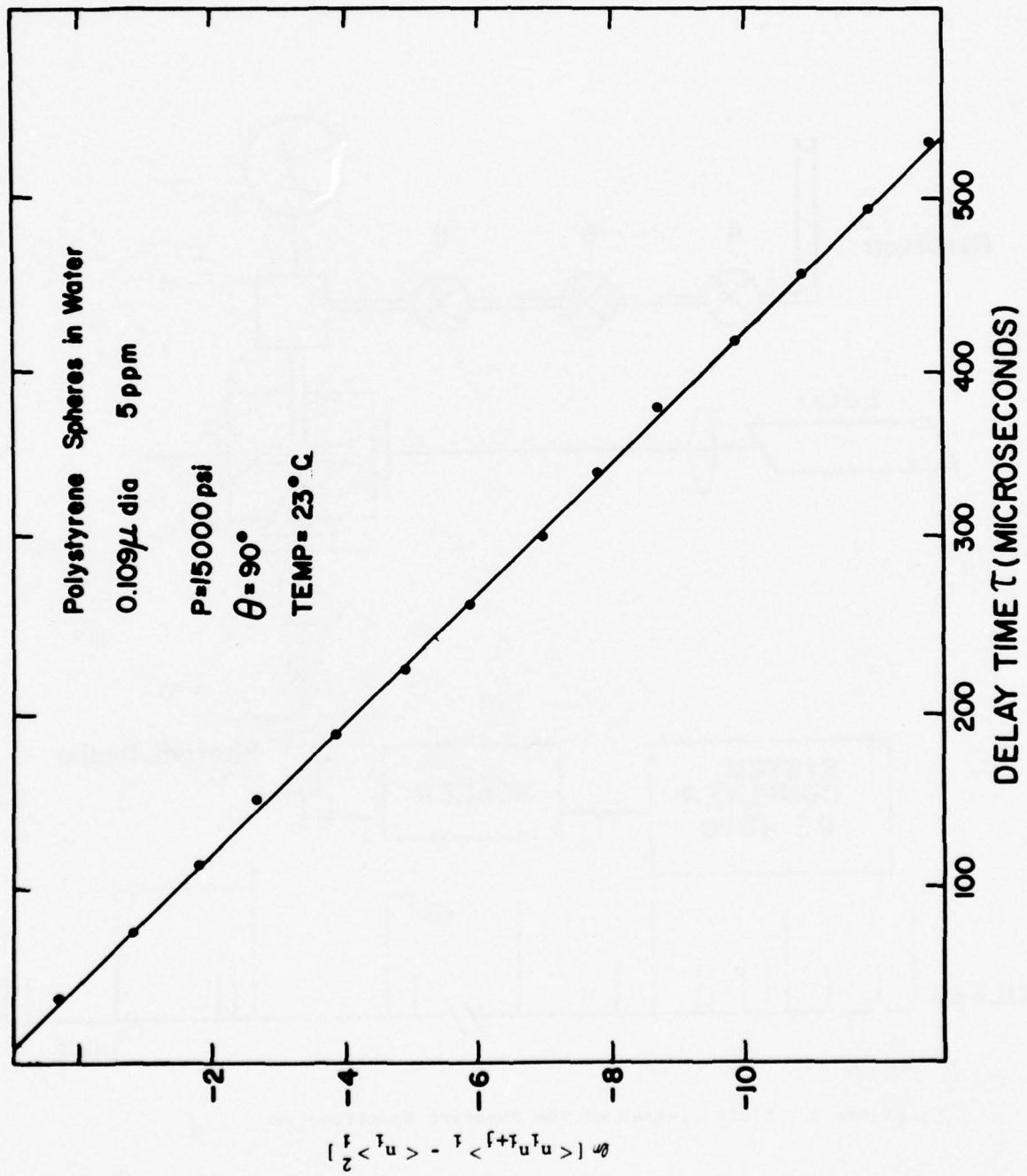


Figure 2 Plot of $\ln [\langle n_i n_{i+j} \rangle_i - \langle n_i \rangle_i^2]$ vs. Delay Time $\tau_j$.

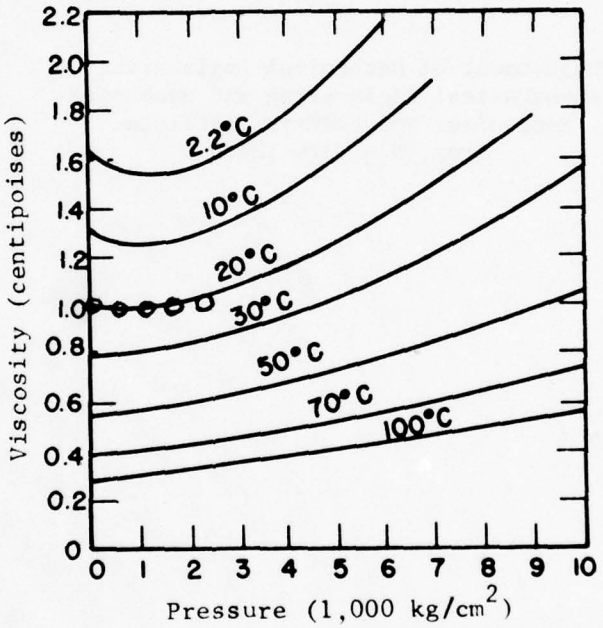


Figure 3 Viscosity of Water vs. Pressure.

APPENDIX B

# THE HIGH FREQUENCY LIMITING BEHAVIOR OF POLYMER SOLUTIONS

In-Young Koh and Meyer H. Birnboim

Department of Mechanical Engineering,
Aeronautical Engineering and Mechanics
Rensselaer Polytechnic Institute
Troy, New York 12181

ABSTRACT

It has been shown experimentally by various investigators that the dynamic viscosity of a dilute polymer solution in the limit of high frequency does not become the viscosity of the solvent. To study this limiting behavior, a high frequency surface delay line has been developed for measurement of $G'_\infty$ and $\eta'_\infty$ in the range from 2 MHz to 40 MHz. Details and equations for this device are described herein. Also the special data acquisition technique required to extract phase/amplitude information from RF pulses is described.

Three Newtonian fluids, NBS oil D, NBS oil J and NBS oil L are used to obtain calibration curves which confirm the theoretical analysis. In addition data is presented on one viscoelastic fluid, NBS oil N.

## 1. Introduction

The viscoelastic response of dilute polymer solutions is usually separated into two parts, the polymer and the solvent contributions. The theories of Rouse, Zimm and others attribute the polymer contribution to internal relaxational modes of the macromolecule, the contribution to the total viscosity at low frequencies drops to zero in the limit of high frequencies. On this basis, one expects the viscosity of the solution to approach the viscosity of the solvent in the limit of high frequencies.

Several investigators have found that this assumption is not borne out experimentally, and the difference between the limiting solution viscosity and that of the solvent has been attributed to internal friction. This interpretation has recently been brought into question by Schrag and the problem remains open.

The experimental techniques that have been used to investigate this phenomenon have primarily been in the frequency range from 0.01 Hz to 10 KHz. This means that it has been necessary to use highly viscous solvents together with the principle of time-temperature superposition to obtain the limiting behavior. Wide frequency range measurements at a single temperature would be desirable to obtain a less ambiguous interpretation of results.

In this paper we describe a device and method for measuring the viscoelastic response of low viscosity liquids in the frequency range 2 MHz to 40 MHz.

The device consists of a glass plate in which a shear wave is propagated between the ends, while the liquid is in contact with the major surfaces. The transverse mode of vibration, called the Meitzler mode, is the same mode as was used by Meeker and Meitzler in an aluminum strip delay line, and was subsequently applied by Hunston and Meyers to polymer solutions. The technique here differs

from the high frequency technique of McSkimin in that the wave propagates in the plane of the solid/liquid interface instead of at a normal or oblique incidence to the interface as in the two methods of McSkimin.

## 2. Description of Apparatus

### a) The Surface Delay Line

The geometry of the fused silica surface delay line is seen in Fig.1. A transverse wave (Meitzler mode) polarized in the y-direction is propagated in the z-direction. Piezoelectric ceramic driving and response transducers of center frequency 25 MHz, are fixed at $z = 0$ and $z = \ell$, respectively. The line length $\ell = 7.62$ cm and thickness $2b = 0.158$ cm. The liquid is in contact with the major surfaces at the interface $x = \pm b$. The beam (transducer) width is 1.9 cms, and the width of the line is 5.08 cm. The thickness of liquid layer for the data reported here is 0.025 cm. The line is isolated from its polycarbonate case by O-rings, and has a flow through arrangement for filling.

The coupled wave solution* for displacement in the y-direction u, in the solid and in the liquid are respectively given by:

$$u_s(x,z,t) = H_s \exp\left[-i\left(\frac{\omega^2}{V^2} - i\,\frac{\omega Z^*}{b\rho V^2}\right)^{\frac{1}{2}} z + i\omega t\right] \cos\left(\frac{i\omega Z^*}{b\rho V^2}\right)^{\frac{1}{2}} x \qquad (1)$$

$$u_L(x,z,t) = H_L \exp - \left[-i\left(\frac{\omega^2}{V^2} - i\,\frac{\omega Z^*}{b\rho V^2}\right)^{\frac{1}{2}} z + i\omega t\right] \exp\left[-\,i\,\frac{\omega\rho_L}{Z^*}\,x\right] \qquad (2)$$

Through Eq. (1), the difference in attenuation $\Delta A$ and in phase $\Delta B$ of the wave measured at $z = \ell$ in the absence and in the presence of liquid can be related to the mechanical impedance $Z^*$ of the liquid by:

---

*Complete equations developed in the Appendix are not included here.

$$\Delta A + i\Delta B = \frac{1}{2\rho bV} Z^* \qquad (3)$$

where $\rho$ and $\rho_L$ are the density of the solid and the liquid and V is the velocity in the solid without liquid.

The mechanical impedance $Z^* \equiv R + iX$ is related to the dynamic shear moduli $G^* \equiv G' + iG'' \equiv G' + i\omega\eta'$ by:

$$\rho_L G' = R^2 - X^2 \; ; \quad \rho_L G'' = 2RX \qquad (4)$$

For a Newtonian liquid of viscosity $\eta$, $G' = 0$, thus

$$R = X = \left(\frac{\rho_L \omega \eta}{2}\right)^{\frac{1}{2}} \qquad (5)$$

b) Pulse Technique and Data Acquisition

A cross-correlation method for measuring phase shift and amplitudes of radio frequency (RF) continuous wave signals, called the methof of walking frequencies, has been described previously (1). Herein this method is extended to phase/amplitude measurements on pulsed RF echoes.

As is seen in Fig.2, a 1 MHz crystal clock is used: to drive the synthesizer to produce the frequency of f MHz, to drive a programmable clock to produce the pulse P every 40 μs, and to drive a snap diode which on mixing with P produces a very fast trigger pulse T every 40 μs. The RF drive pulse A of frequency f is produced every 1280 μs (32 × 40 μs) by mixing the synthesizer output with the d.c. pulse Q of nominal width 25 μs, that has been appropriately delayed. The response signals (echoes) B, from the delay line output are then sampled every 40 μs by the trigger pulse T. The length of line is such that the interval between successive echoes is nominally 40 μs; thus the drive delay (above) is adjusted so that echoes and sampling overlap.

The output of the sample and hold amplifier is then measured by the analog to digital converter every 40 μs and stored into the memory of the

computer. In order that a complete and separate sinusoidal wave is developed in the memory from each echo, the synthesizer must always be set to a walking frequency. A walking frequency f is given by:

$$f \equiv f_N + f = \frac{N}{T} + \frac{1}{32nT} \tag{6}$$

where $f_N$ corresponds to any commensurate frequency (every 25 KHz since $T = 40\ \mu s$ and $N = 1,2,3 \ldots$) and if we choose $n = 625$ memory locations to correspond to $2\pi$ radians, then $\Delta f = 1.25$ Hz. Thereby for each echo one sinusoidal wave is reconstructed in 625 locations, and, if they existed, 32 echoes could be measured.

By the cross-correlation techniques described elsewhere (2) the relative phase and amplitude between any one echo and another echo or drive signal can be computed.

## 3. Experimental Results and Conclusions

As can be seen from Eq. (3) we expect linear relations between $\Delta A$ and R and $\Delta B$ and X, with the proportionality constant indicated. Alternatively calibration curves can be obtained by using Newtonian fluids for which R and X can be calculated by Eq. (5), from steady-state viscosity, frequency and density. Such calibration curves are shown in Fig.3. The superposition of these various liquids and frequencies establish the validity of the method.

One fluid, NBS oil N, is shown in Fig.4 to be viscoelastic in this frequency range.

## 4. Acknowledgment

This work was supported, in part, by the Air Force Systems Command, Air Force Materials Laboratory under Contract No. F33615-75-C-5105.

## REFERENCES

1. Birnboim, M.H. and Koh, In-Young, Bull. Amer. Physics Soc., 18, 318 (1973).

2. Birnboim, M.H., Burke, J.S., Anderson, R.L., Proc. Fifth Int'l. Cong. Rheology, 11, 409 (1969).

3. McSkimin, H.J., J. Acoust. Soc. Am., 24, 355 (1952).

4. Meeker, T.R. and Meitzler, A.H., in "Physical Acoustics," vol. IA, Mason, W.P., ed., Academic Press, 1964.

5. Hunston, D., Ph.D. Dissertation, 1969, Kent State University.

6. Miller, J.W. and Schrag, J.L., Macromolecules, 8, 361 (1975).

## FIGURE CAPTIONS

Figure 1 — Delay line configuration, where $\vec{k}$ is the propagation vector, $\vec{u}$ is the particle displacement, A and B are the drive and response RF pulses.

Figure 2 — Block diagram of electronics. The output of the analog to digital converter CPU, transfers data directly into *computer memory*.

Figure 3 — Calibration curves for liquid mechanical resistance and reactance in terms of measured attenuation $\Delta A$ and phase shift $\Delta B$, respectively. Measurements at 3.4, 6.0 and 14.5 MHz.

Figure 4 — Viscoelastic behavior of NBS oil N.

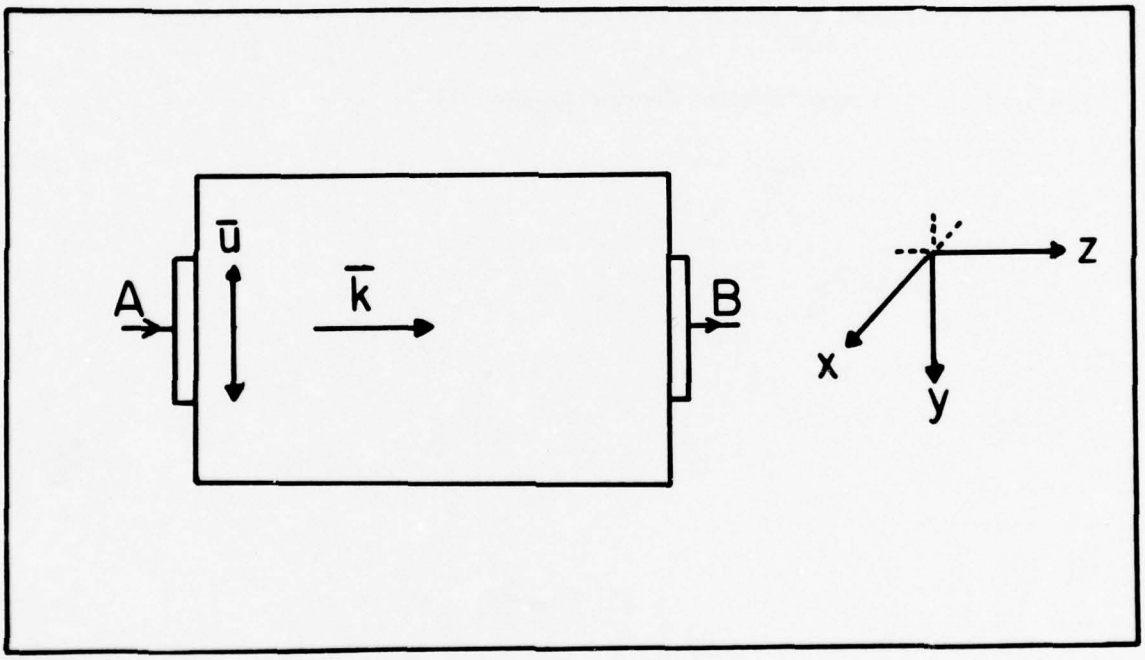


Figure 1 Delay Line Configuration where $\vec{k}$ is the Propagation Vector, $\vec{u}$ is the Particle Displacement, A and B are the Drive and Response RF Pulses

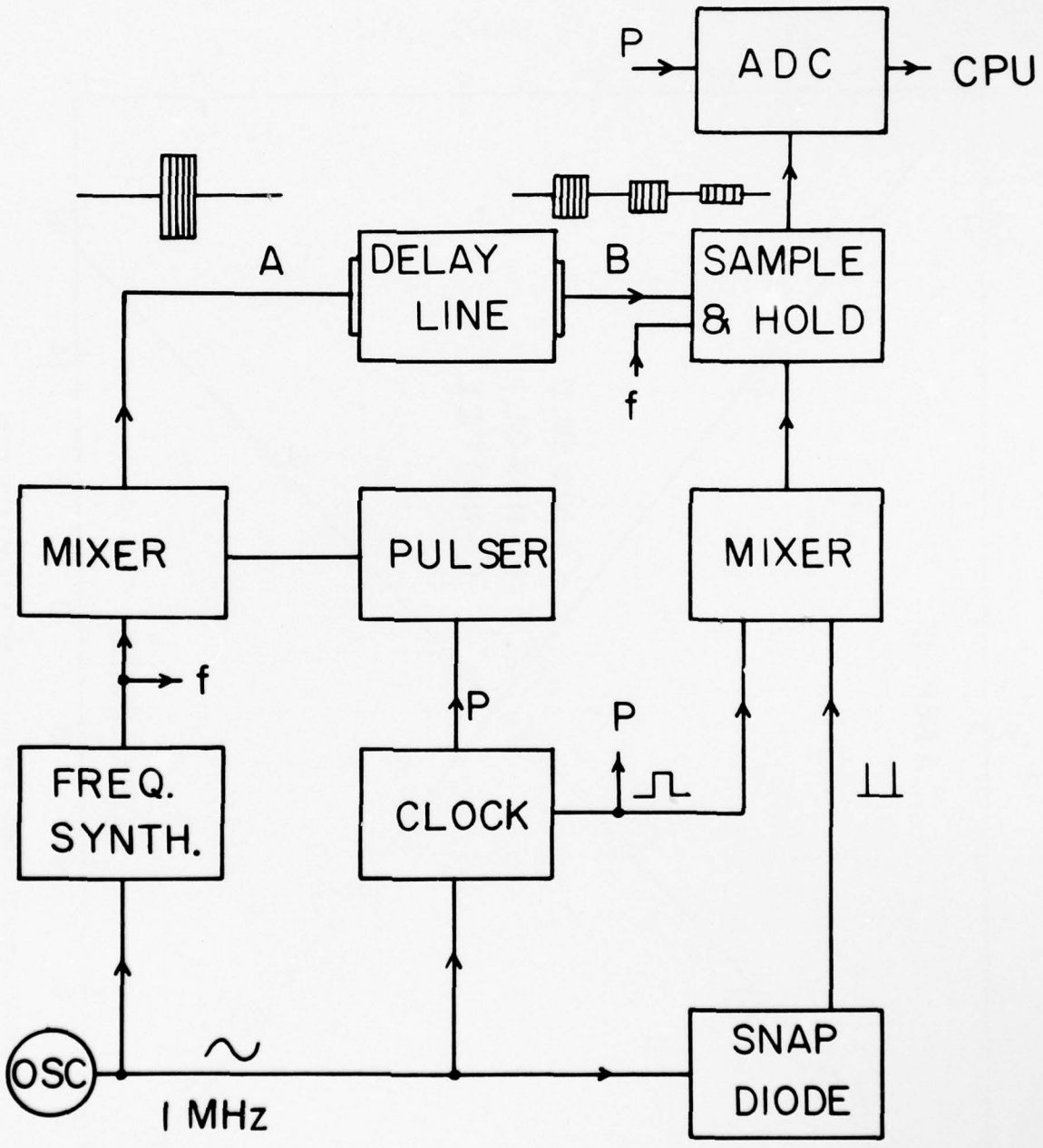


Figure 2 Block Diagram of Electronics. The output of the analog to digital converter CPU, transfers data directly into computer memory.

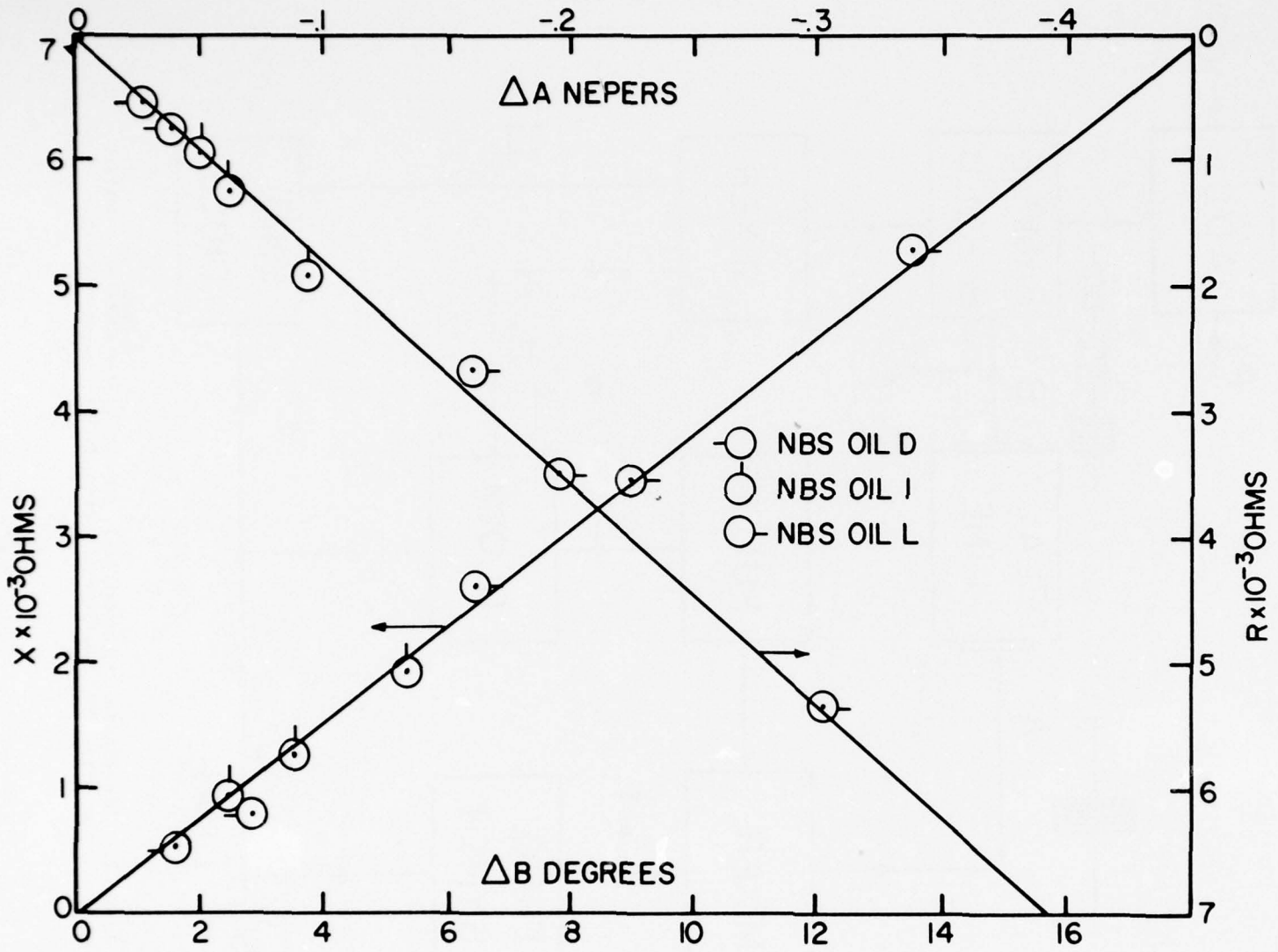


Figure 3 Calibration Curves for Liquid Mechanical Resistance and Reactance.

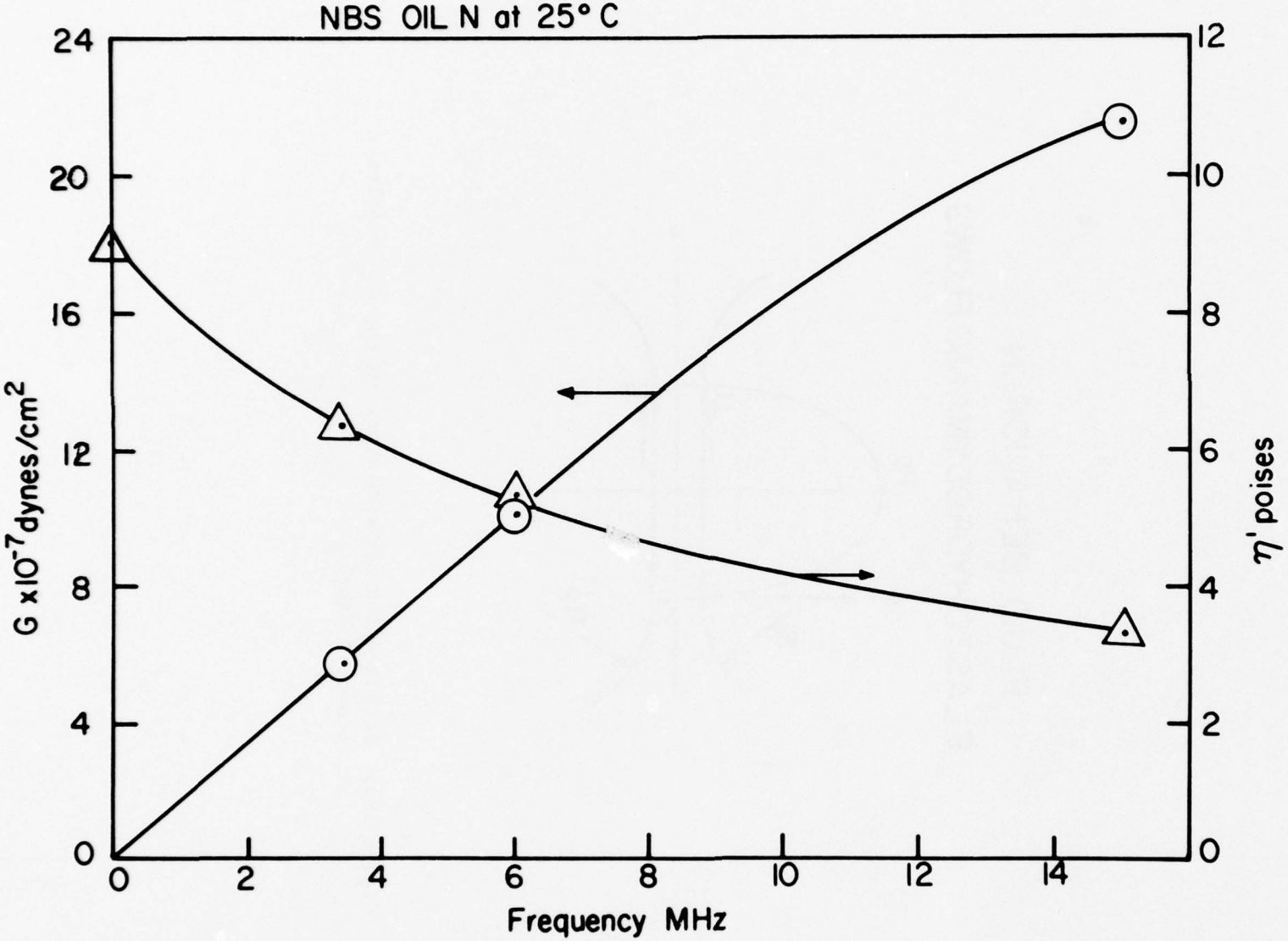


Figure 4 Viscoelastic Behavior of NBS oil N

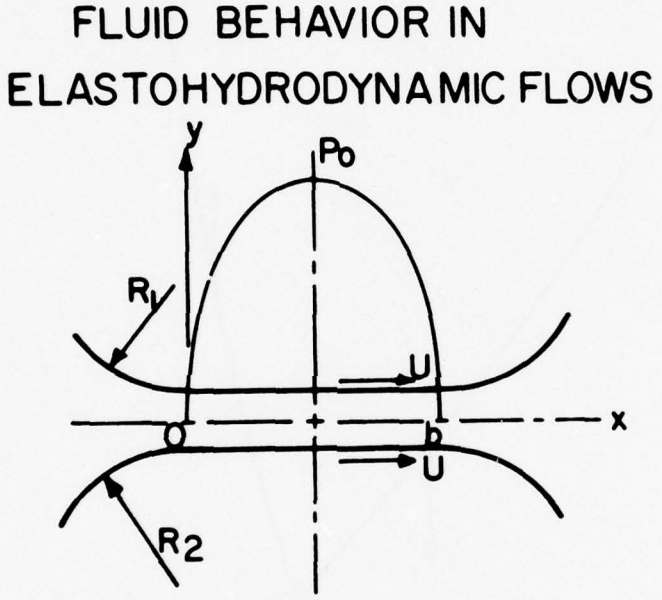


Figure 1(a) Stress/Deformation History in the EHD Problem (Contact Zone)

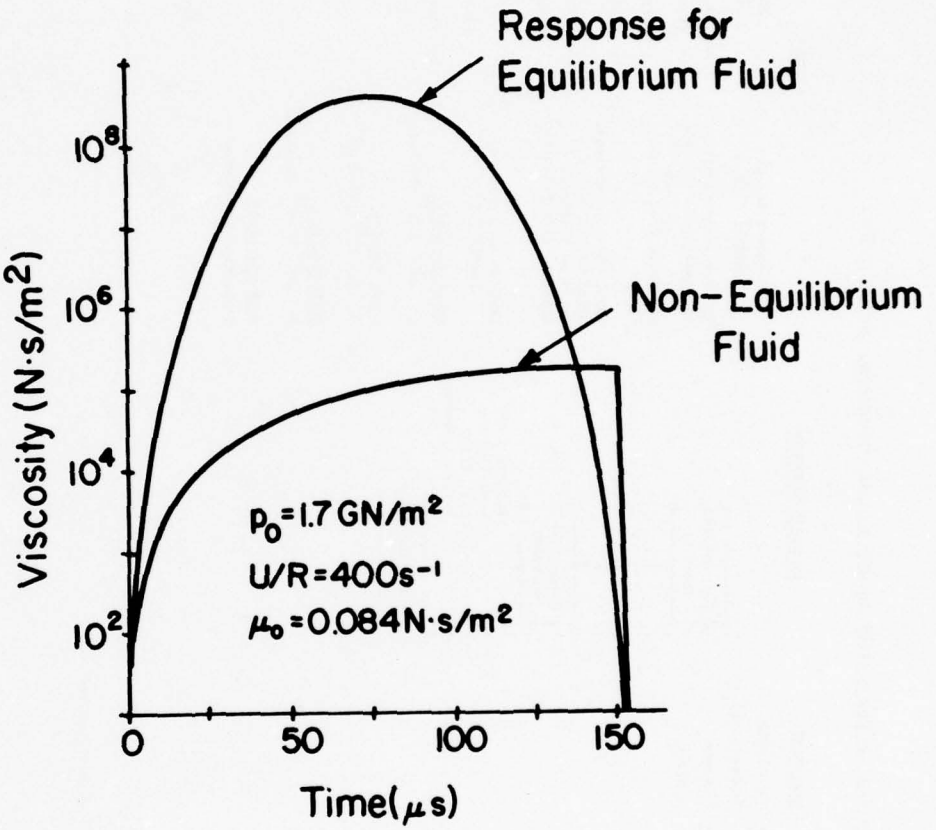


Figure 1(b) Stress/Deformation History in the EHD Problem

PROPERTIES OF THE LIQUID STATE FOR BOTH LOW AND HIGH MOLECULAR WEIGHT FLUIDS

**EXPERIMENTAL TECHNIQUES***

I. Wide Frequency Range Viscoelastic for Mechanical Relaxation Spectroscopy:

- ◒ Magnetic Suspension Viscometer DC → $10^3$ Hz
- ● Multiple Lumped Resonator 50 - 5000Hz
- ● Mason Torsion Crystals 20 - 200KHz
- ● Torsional Wire Delay Line 500KHz - 4MHz
- ◒ Meitzler Mode Surface Delay Line 0.5 - 50MHz
- ● Bragg Diffraction Cell (Bulk Modulus) 0.5 - 50MHz

II. Laser Light Scattering Techniques for Optical Relaxation Spectroscopy:

- ● Rayleigh Scattering (Quasi-elastic Light Scattering)
- ● High Pressure Cell for Scattering - Includes High Pressure Viscosity by Diffusion of Spheres
- ◒ Brillouin Scattering
- ○ Depolarized Scattering
- ○ Rayleigh Wing Scattering

**VARIABLES**

- Time Scale
- Temperature
- Pressure
- History

**MATERIAL RESPONSE**

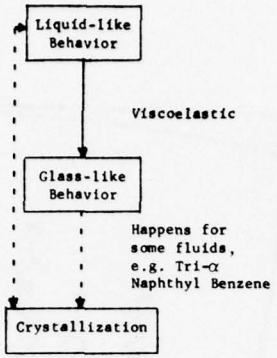


**NEEDS**

**Phenomenological Description**

WLF Time/Temperature Superposition Principle

Doolittle Free Volume Theory

Basic Three-dimensional Viscoelastic Theory Based on Boltzmann Superposition Principle

[Macroscopic Physical Parameters]

Shear Viscosity

$\eta$: $10^{-1} \rightarrow 10^{12}$ poises

Shear Modulus

G: $0 \rightarrow 10^{11}$ dynes/cm$^2$

Bulk Modulus

B: $10^{10} \rightarrow 10^{12}$ dynes/cm$^2$

Bulk Viscosity

Structural Relaxation

**Microscopic Model Interpretation**

Relevant Molecular Theories:

- Free Volume Theory
- Gibbs Statistical Model
- Turnbull
- Landau-Placzek
- Rouse/Zimm/Kirwood/Fixman
- Zwanzig
- Litovitz
- Fluery
- ⋮

*All of above interface existing on-line computer data acquisition system.

● Currently available in Viscoelasticity Laboratory.

◒ Under development in Viscoelasticity Laboratory.

○ Proposed acquisition to Viscoelasticity Laboratory.

Figure 2 Survey of Properties of the Liquid State

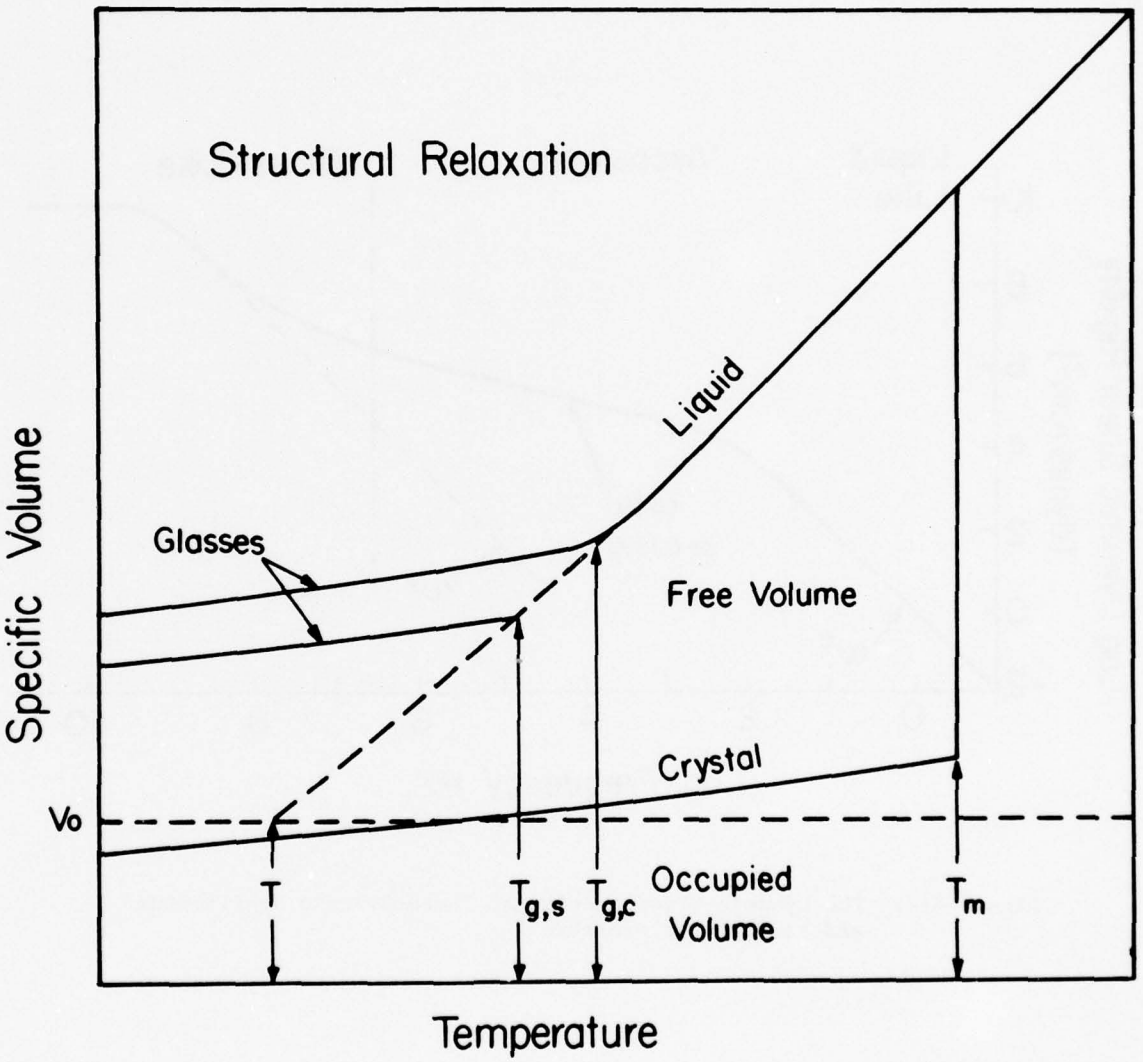


Figure 3 The Volume-Temperature Curves with Reference to: Equilibrium, Nonequilibrium, Glass/Liquid to Glass Transition

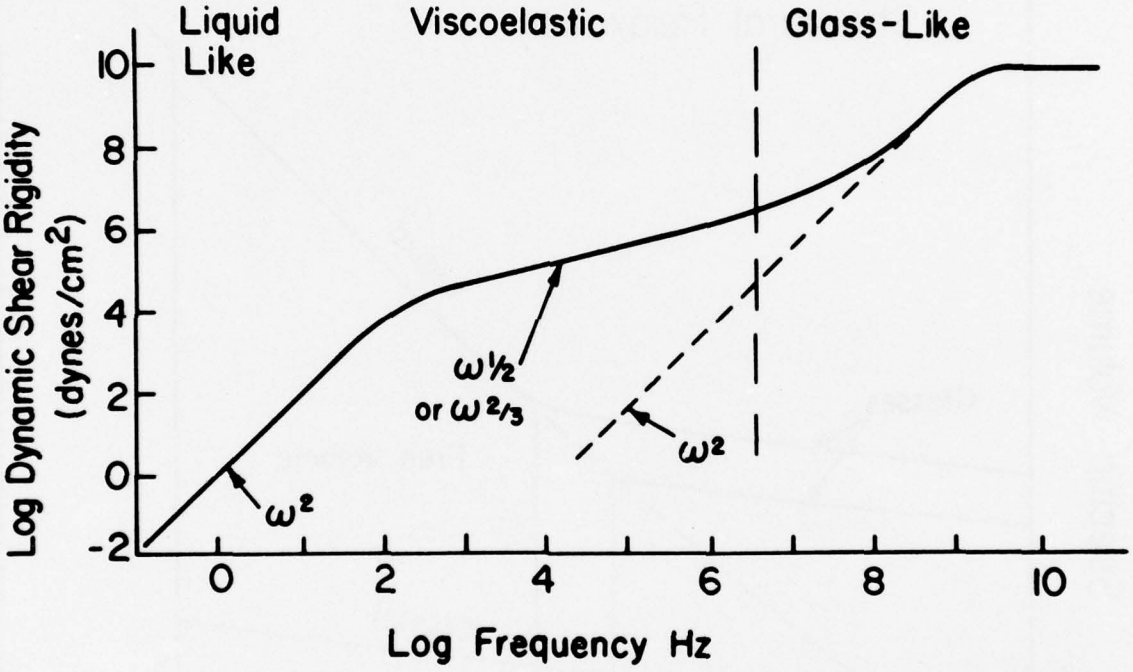


Figure 4(a) The Dynamic Shear Modulus at Thermodynamic Equilibrium and Atmospheric Pressure

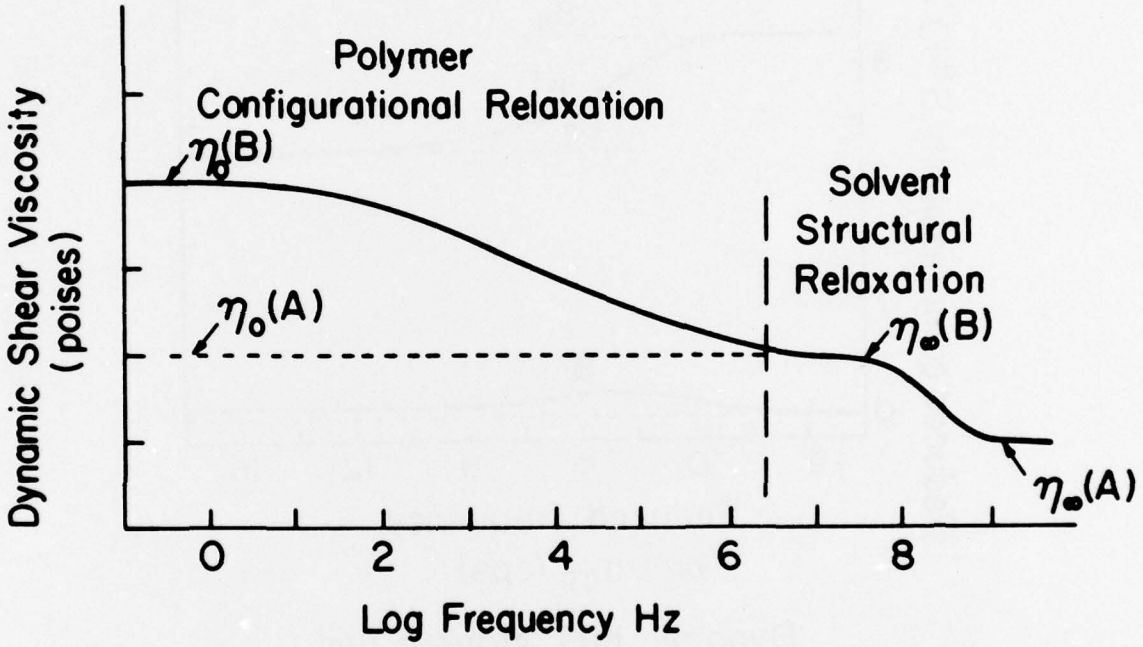


Figure 4(b) The Dynamic Shear Viscosity at Thermodynamic Equilibrium and Atmospheric Pressure

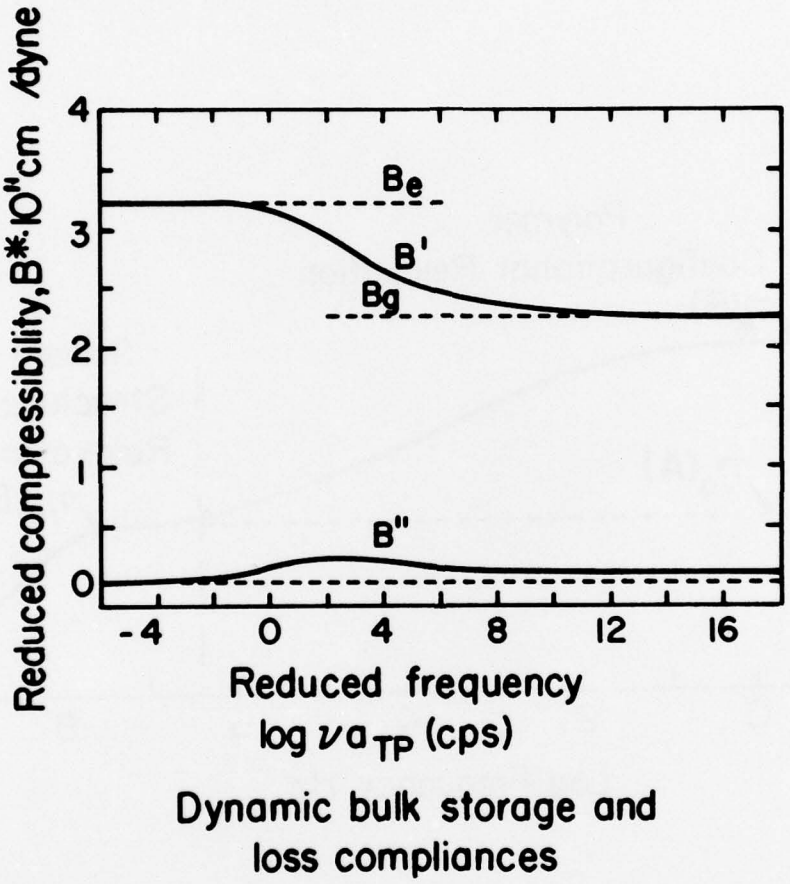


Dynamic bulk storage and loss compliances

Figure 5(a) The Dynamic Compressibility: Viscosity and Modulus

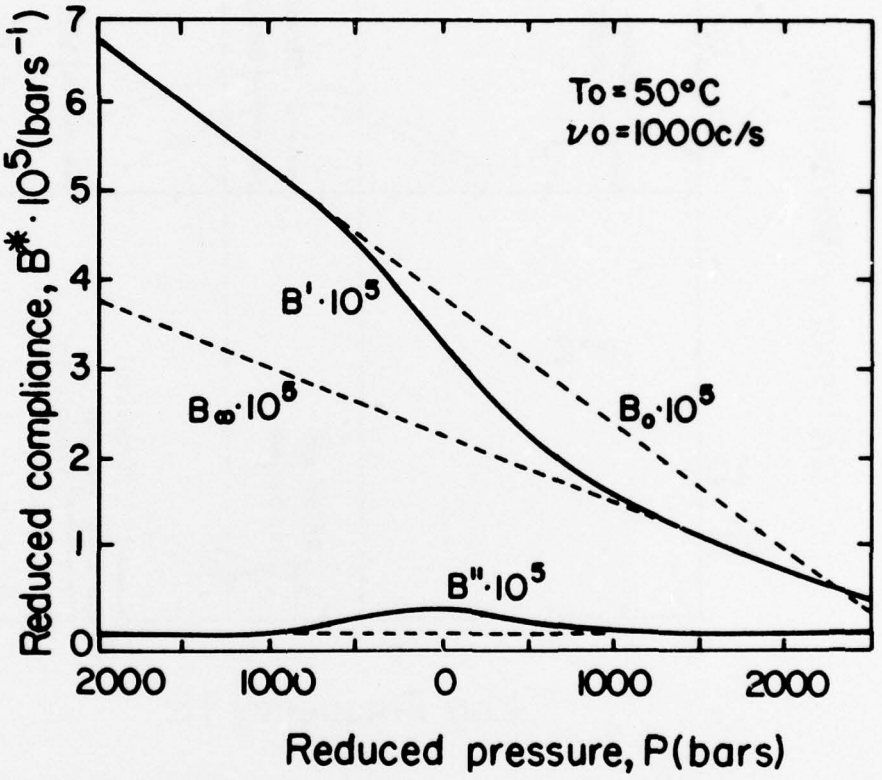


Figure 5(b) The Dynamic Compressibility: Viscosity and Modulus

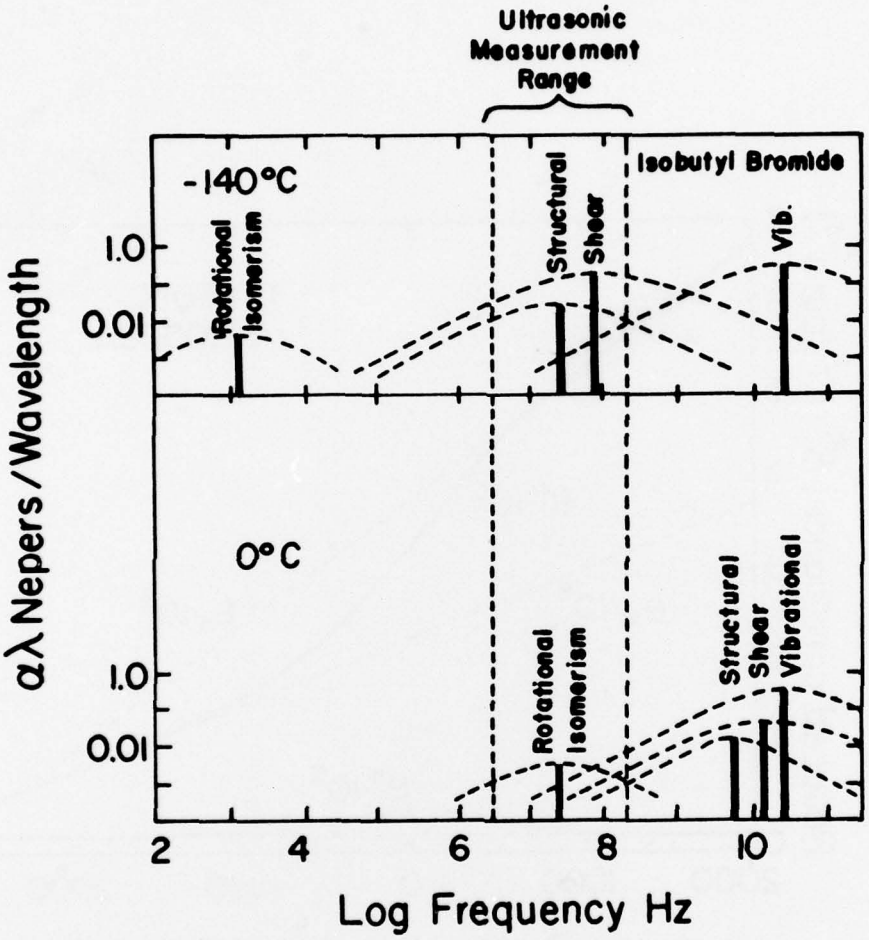


Figure 6 Summary of Mechanical Relaxation Spectra

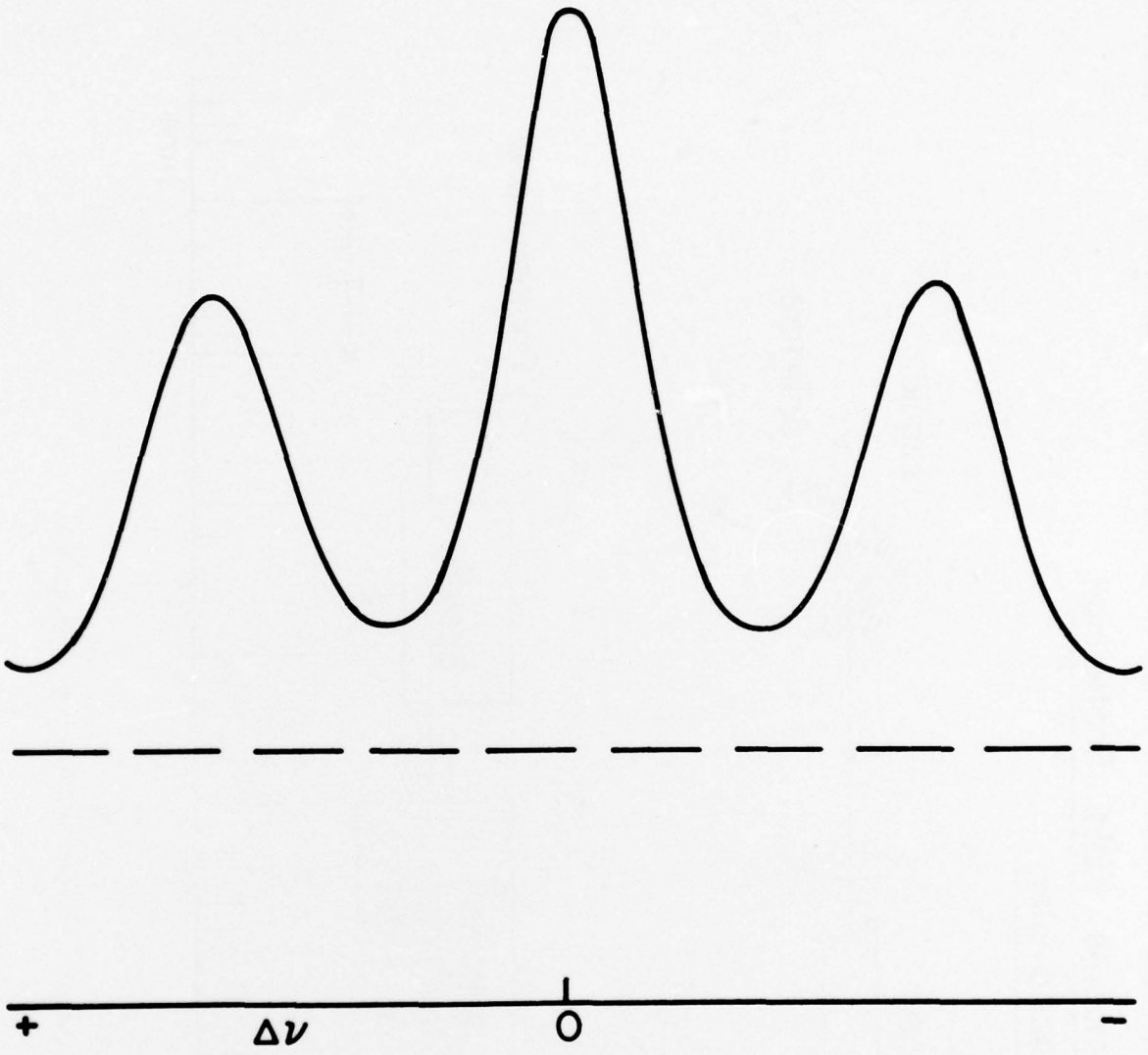


Figure 7 Light Scattering Spectrum with Rayleigh (Central and Brillouin Peaks for Benzene

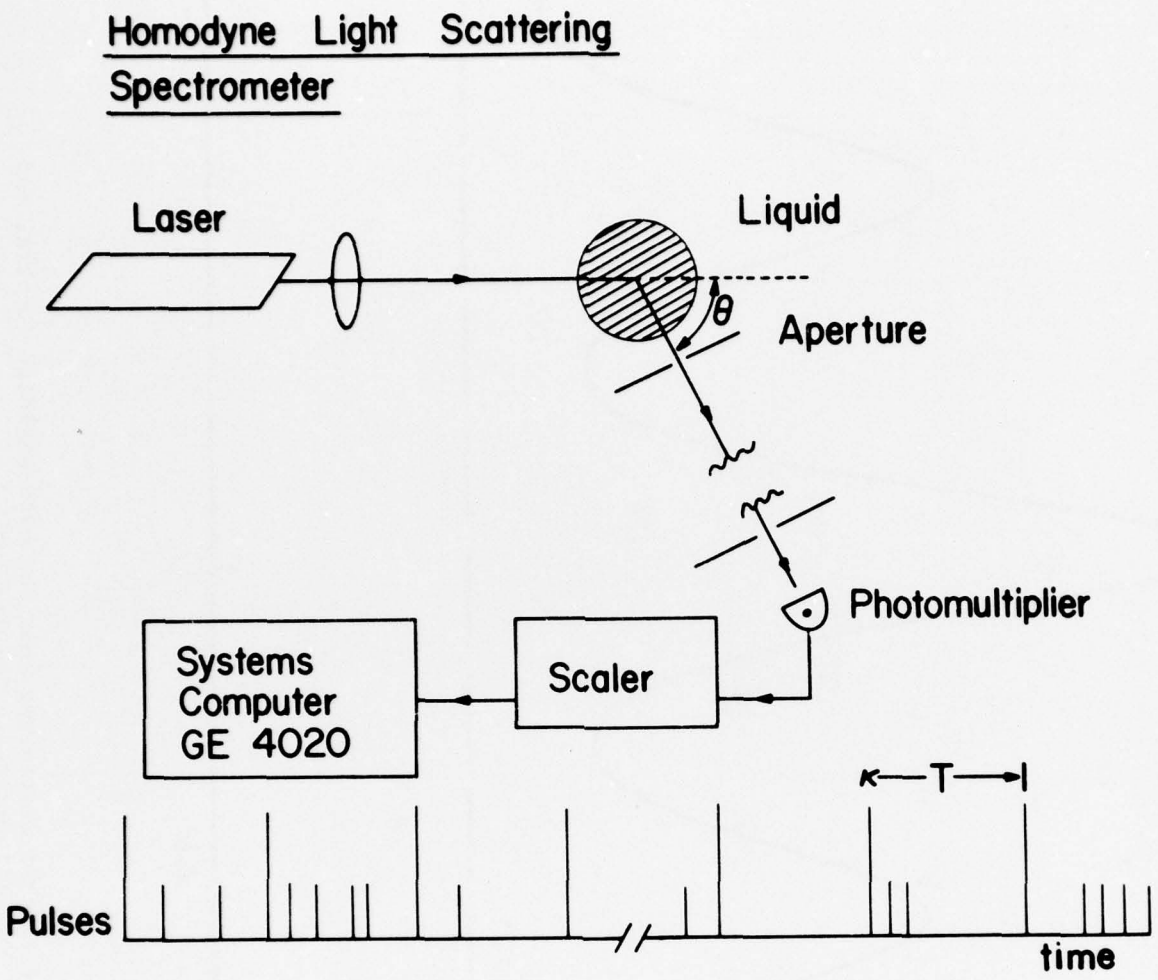


Figure 8 Light Scattering Apparatus

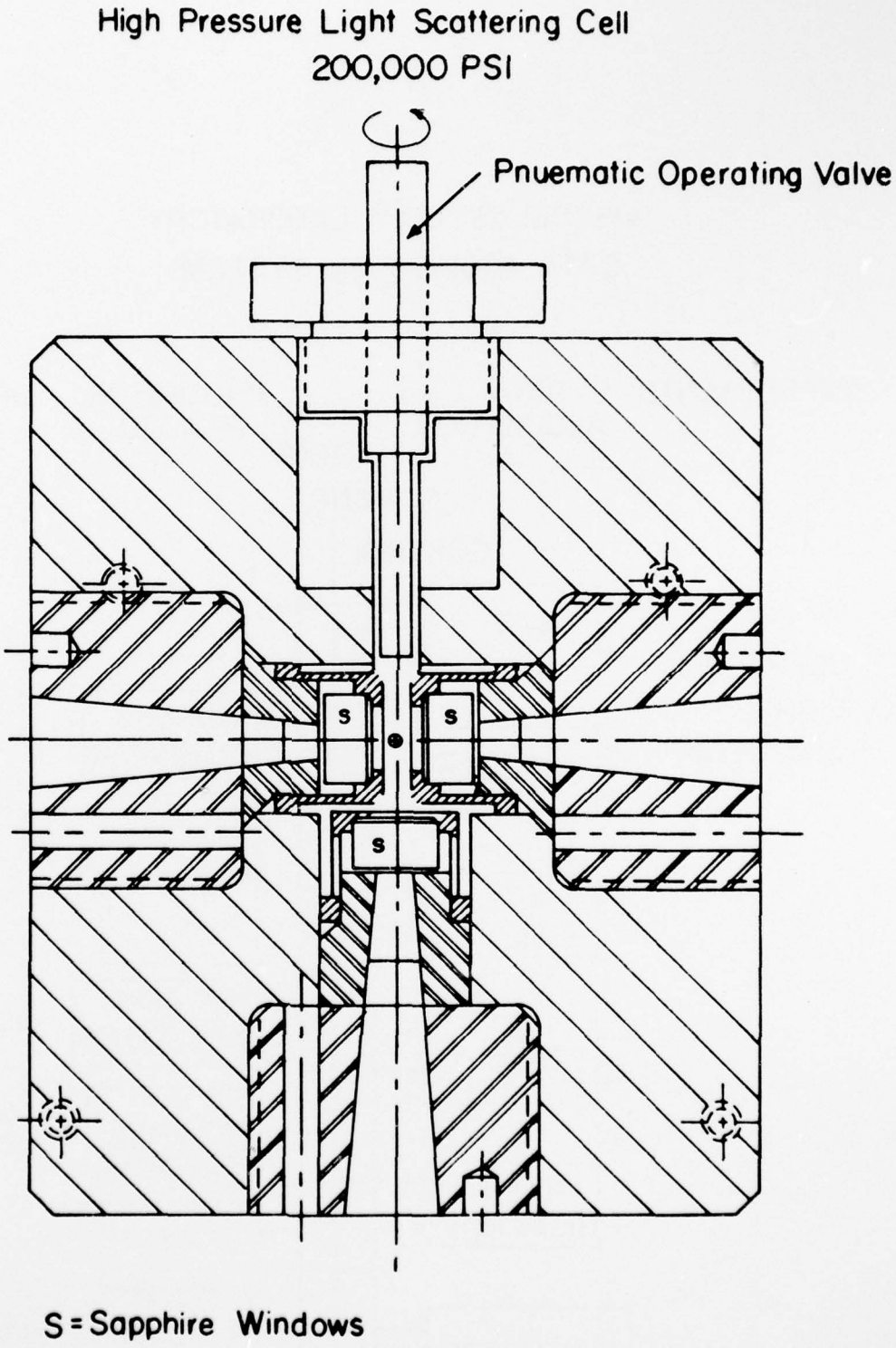


Figure 9 The New High Pressure Cell

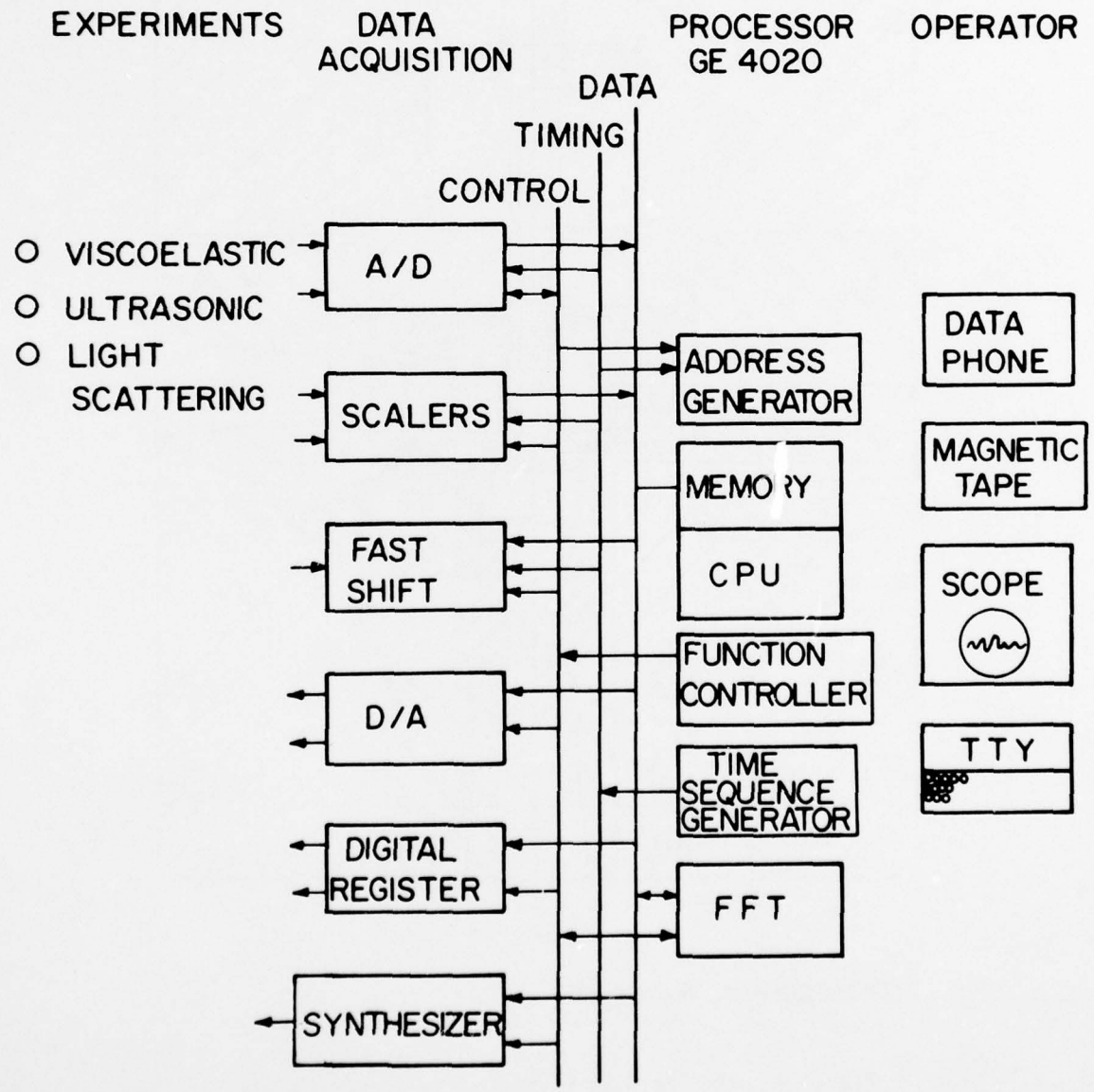


Figure 10 Viscoelasticity/Light Scattering Data Acquisition System

Diamond Cell

Optical Geometry

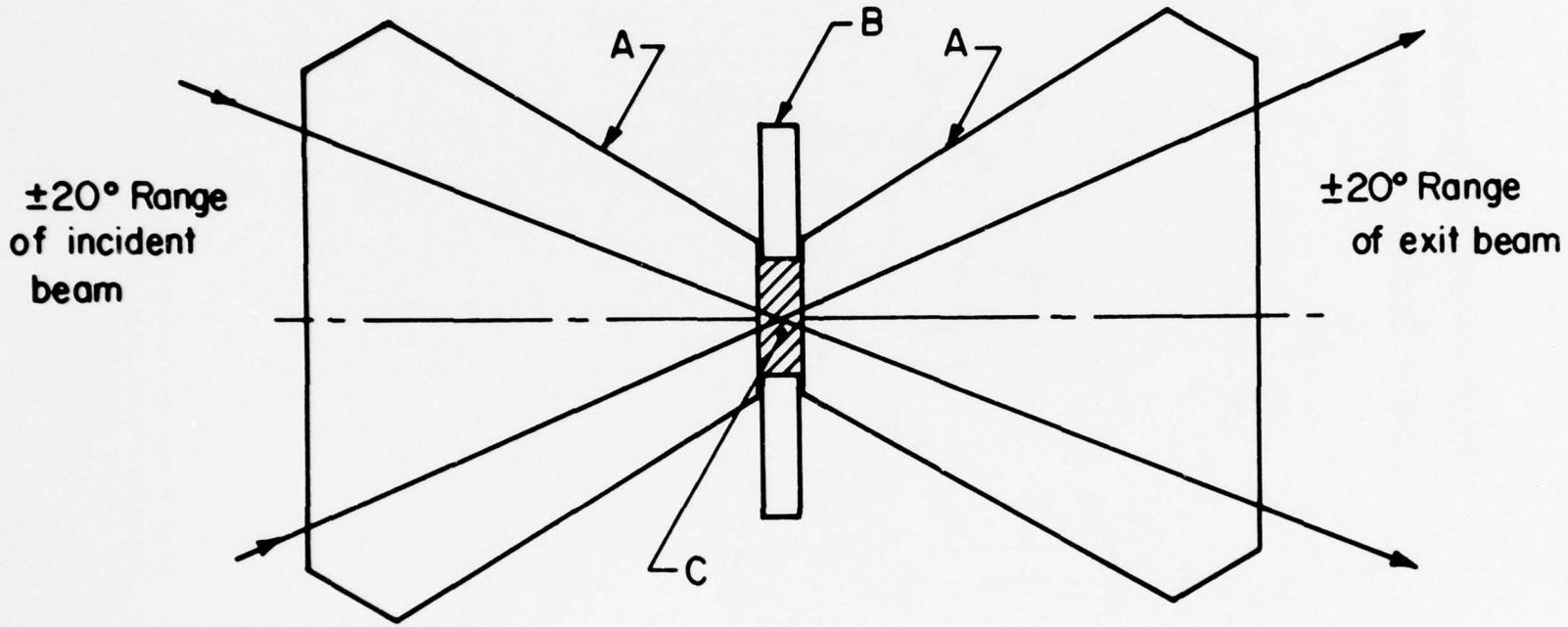


Figure 11 Diamond Cell Optics
A - Diamonds; B - Spacer; C - Liquid Sample
Note that refraction corrections have been neglected

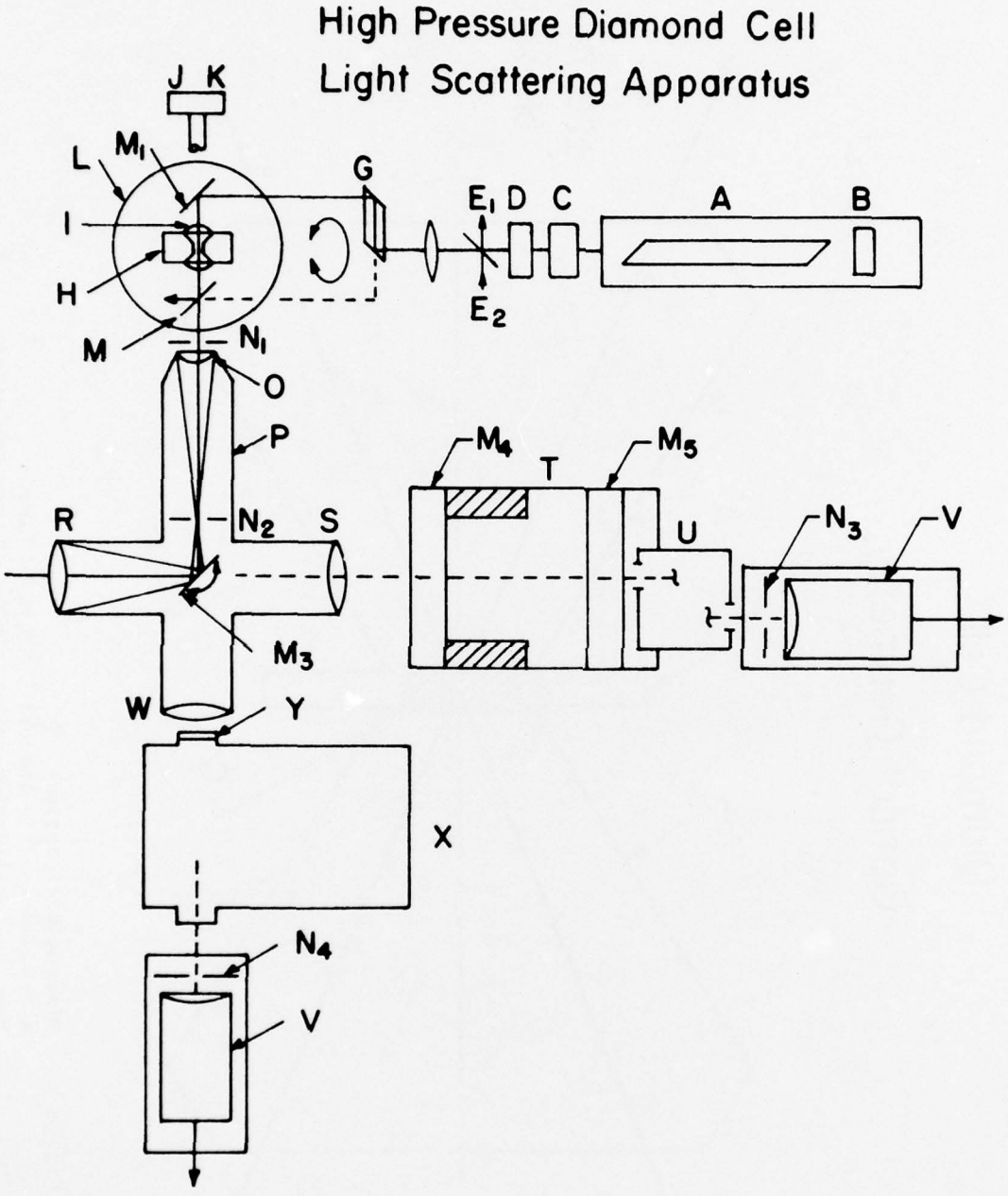


Figure 12 High Pressure Diamond Anvil Cell Light Scattering Apparatus (see page 63 for caption)

Figure 12 - Captions

A - Argon ion laser, B - Single frequency etalon, C - Polarization rotator, D - Spatial filter, E - Partial (5%) reflector - for beam intensity monitor or alternately $E_2$ entrance point for HeNe (red) laser (second source), F - Lens to focus beam into "waist" diameter of 50 microns, G - Prism. Rotate 180° to displace beam from "forward to backward scattering" illumination, H - Diamond anvil cell, I - Cell clamp with cell orientation adjustment, J - Pressure adjustment screw (only partly shown), K - Pneumatic impact relay, (not shown), L - Primary goniometer to adjust scattering angle, $M_1$ - Mirror for beam steering in forward scattering regime, $M_2$ - Partially reflecting mirror for beam steering in back scattering regime, N - Adjustable slits or apertures, O - Microscope objective, P - Three port microscope body attached to Table L, $M_3$ - Rotatable and removable mirror for beam steering to R, S; R - Eyepiece or Vidicon port, S - Lens, T - Piezoelectrically driven Fabry Perot interferometer of adjustable free spectral range, U - Multipass corner cube reflector and an Iodine filter (not indicated), V - Photomultiplier, W - Lens, X - Double grating spectrometer, Y - Filter for fluorescence.

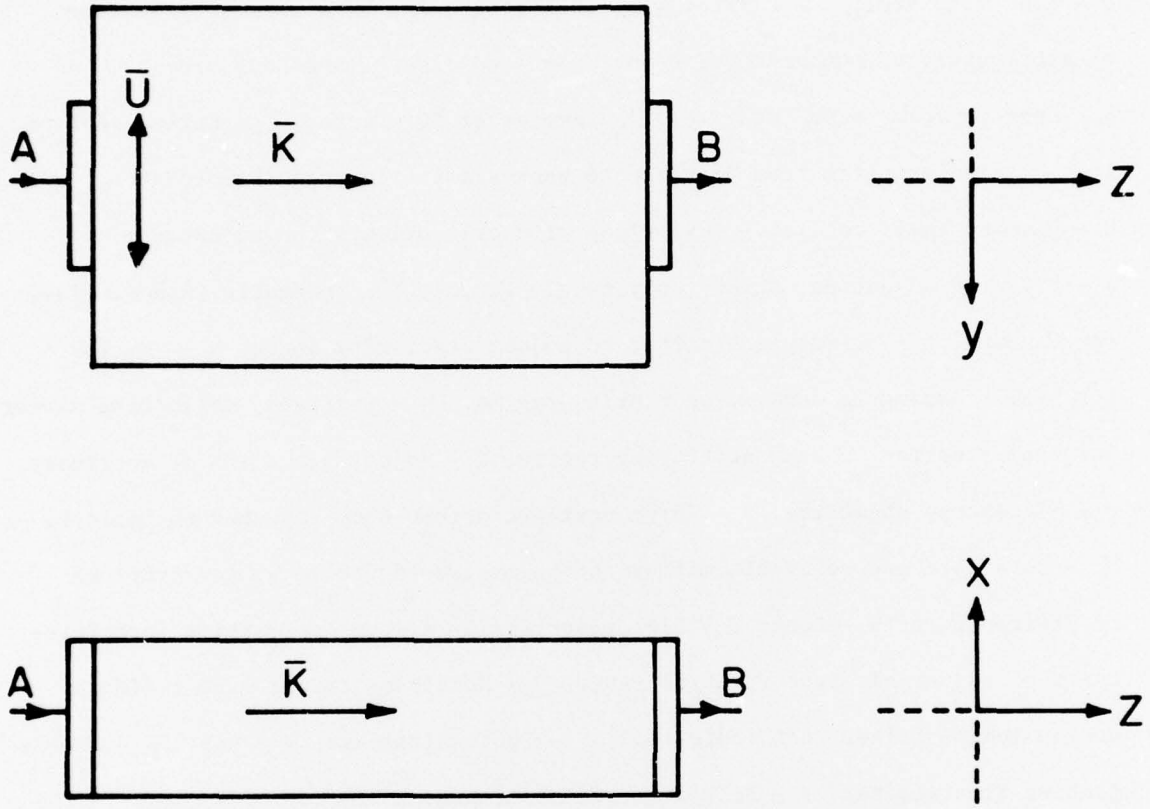


Figure 13 Delay Line

## REFERENCES


1. D. Dowson and G.R. Higginson, Elastohydrodynamic Lubrication, Pergamon Press, New York 1966.

2. T.E. Tallian, Elastodynamic Hertzian, Mechanical Engineering, p.14, November 1971.

3. H. Christensen, Elastohydrodynamic Theory of Spherical Bodies in Normal Approach, J. Lub. Tech., 92, 145 (1970).

4. E.G. Trachman, The Short-Time Viscosity Behavior of a Lubricant in a Hertzian Pressure Zone, J. Lub. Tech., Trans. ASME, 74 Lub-8.

5. J. Jakobsen and W.O. Winer, High-Shear Stress Behavior of Some Representative Lubricants, ASLE Preprint, 74 Lub-41.

6. W.R. Jones, Jr., R.L. Johnson, W.O. Winer and D.N. Sanborn, Pressure-Viscosity Measurements for Several Lubricants to $5.5 \times 10^8$ N/m$^2$ and 149°, *NASA Technical Note* NASA TN D-7736, 1974.

7. D.J. Plazek and J.H. Magill, Physical Properties of Aromatic Hydrocarbons IV. An Analysis of the Temperature Dependence of the Viscosity and the Compliance of 1, 3, 5 Tri-$\alpha$-naphthylbenzene, J. Chem. Phys., 49, 3678 (1968).

8. A.K. Doolittle, Studies in Newtonian Flow. III. The Dependence of the Viscosity of Liquids on Molecular Weight and Free Space (in Homologous Series), J. Appl. Phys., 23, 236 (1952).

9. M. Cohen and D. Turnbull, Molecular Transport in Liquids and Glasses, J. Chem. Phys., 47, 2185 (1967).

10. J.H. Gibbs and E.A. DiMarzio, Nature of the Glass Transition and the Glassy State, J. Chem. Phys., 28, 373 (1958).

11. A.J. Barlow and E. Erginsav, Viscoelastic Relaxation in a Series of Short Chain Polydimethyl Siloxanes, J. Acoust. Soc. Am., 56, 83 (1974).

11a. G. Harrison and E.G. Trachman, The Role of Compressional Viscoelasticity in the Lubrication of Rolling Contacts, J. Lub. Tech., Trans. ASME, F94, 306 (1972).

12. R.S. Marvin and J.E. McKinney, Volume Relaxation in Amorphous Polymers, Physical Acoustics, Vol.IIB, p.165, Warren P. Mason, ed., Academic Press, 1965.

13. J. Lamb, Thermal Relaxation in Liquids, Physical Acoustics, IIA, 203, Warren P. Mason, ed., Academic Press, 1965.

14. T.A. Litovitz and C.M. Davis, Structural and Shear Relaxation in Liquids, Physical Acoustics, IIA, 281, Warren P. Mason, ed., Academic Press, 1965.

15. J.D. Ferry, Viscoelastic Properties of Polymers, John Wiley & Sons, 1970.

16. H.Z. Cummins and R.W. Grammon, Rayleigh and Brillouin Scattering in Liquids: The Landau-Placzek Ratio, J. Chem. Phys., 44, 2785 (1966).

17. P.A. Fleury, Light Scattering as a Problem of Phonons and other Excitations, Physical Acoustics, Vol.VI, p.2, Warren P. Mason, ed., Academic Press, 1970.

18. J.D. Barnett, S. Block and G.T. Piermarini, An Optical Fluorescence System for Quantitative Pressure Measurement in the Diamond-Anvil Cell, Rev.Sci. Inst., 44, 1 (1973).

19. J.L. Lauer and M.E. Peterkin, Analysis of Infrared Spectra of Fluid Film in Simulated EHD Contacts, ASLE Preprint 74 LUB-34.

20. G.R. Paul and A. Cameron, An Absolute High Pressure Microviscometer Based on Refractive Index, Proc. Roy. Soc.A, London, 1 (1972).

21. H.Z. Cummins and E.R. Pike, Photon Correlation and Light Beating Spectroscopy, Plenum Press, New York 1974.

22. M.H. Birnboim and H. Weiss, A Novel Method for Viscosity Measurements at High Pressures, Presented in part, American Physical Society.

23. J.F. Dill, P.W. Drake and T.A. Litovitz, The Study of Viscoelastic Properties of Lubricants Using High Pressure Optical Techniques, ASLE Preprint 74 LC-5B-2.

24. H.J. McSkimin, Ultrasonic Methods for Measuring the Mechanical Properties of Liquids and Solids, Physical Acoustics, IA, 271, Warren P. Mason, ed., Academic Press.

25. Modern Very High Pressure Techniques, R.H. Wentorf, editor, Butterworths, 1962.

26. M.A. Lowenstein and M.H. Birnboim, A Method for Measuring Sedimentation and Diffusion of Macromolecules in Capillary Tubes by Total Intensity and Quasi-Elastic Light-Scattering Techniques, Biopolymers, 14, 419 (1975).

27. T.R. Meeker and A.M. Meitzler, in Physical Acoustics, Vol.IA, W.P. Mason, ed., Academic Press 1964.

28. D. Hunston, Ph.D. Thesis, "Determination of Viscoelastic Constants for Polymers,"Chemistry Dept., Kent State University, December 1969.



☆ U. S. GOVERNMENT PRINTING OFFICE: 1976 — 757-067/192